ABSTRACT

TRIVEDI, ISHITA. Uncertainty Quantification and Propagation Methodology for Steady State Safety Analysis of Lead-cooled Fast Reactors. (Under the direction of Dr. Jason Hou and Dr. Kostadin Ivanov).

Current efforts towards development of preliminary designs for Lead-cooled Fast Reactors (LFRs) have demonstrated a need for assessing uncertainty propagation through the reactor system. Safety parameters determined using modern codes have a direct impact from nuclear data uncertainties. Evaluating uncertainties will lead to a better understanding of their impact on LFR core design, and will identify the design safety limits that are reviewed during the licensing process. Here, "Best Estimate Plus Uncertainty" approach is applied to LFR to propagate nuclear data uncertainties through multiple scales of core modelling.

The Monte Carlo code SERPENT-2.0 with implemented Generalized Perturbation Theory (GPT) was used to calculate the sensitivity coefficients of the multiplication factor with respect to nuclide and reaction-dependent nuclear data for fuel assembly models on fuel lattice level. Nuclear data UQ&P was then extended to whole core using Argonne National Lab (ANL) Advanced Reactor Computational (ARC) suite and verified with SERPENT-2.0. In ARC, DIF3D was employed for core modeling and PERSENT was used for sensitivity coefficient calculations. Standard deviations for reactivity feedback coefficients such as doppler, radial expansion and fuel/structure/cooland density were determined.

From initial assessment, main contributors of uncertainty were traced back to a number of common nuclide reaction pairs including U-235 capture, U-238 capture, U-238 elastic, U-238 inelastic, and Pu-239 capture.

Uncertainty Quantification and Propagation Methodology for Steady State Safety Analysis of Lead-cooled Fast Reactors

by
Ishita Trivedi

A thesis submitted to the Graduate Faculty of
North Carolina State University
in partial fulfillment of the
requirements for the degree of
Master of Science.

Nuclear Engineering

Raleigh, North Carolina
2020

APPROVED BY:

_____	_____
Jason Hou	Kostadin N. Ivanov
Committee Co-Chair	Committee Co-Chair

_____
Maria N. Avramova

BIOGRAPHY

Ishita Trivedi was born in India to Ram and Sudha Trivedi. Ishita has a brother, Dr. Harshil Trivedi who is a doctor in Australia, and whom she considers her closest friend. She completed her pre-college education while living in many different countries including, Denmark and Thailand. With an international upbringing, she considers her hometown to be wherever her parents are. Post-secondary, she attended Pennsylvania State University where she received Bachelors of Science in Nuclear Engineering. After that, she received a fellowship to continue graduate school at North Carolina State University in Nuclear Engineering. Outside of work, she enjoys exploring museums, running, learning to cook.

ACKNOWLEDGMENTS

This project is completed with primary guidance from Dr. Jason Hou who also served as the committee co-chair. Additional support was provided by external members Dr. Giacomo Grasso (ENEA), Dr. Nicolas Stauff (Argonne National Lab) and, Dr. Fausto Franceschini (Westinghouse Electric Co.).

Apart from academic guidance, I had a tremendous amount of support from my family and friends. I could not have completed this degree without them. With that, I would like to dedicate this thesis to my brother - Dr. Harshil Trivedi. Thank you Harshil for always being in my corner.

TABLE OF CONTENTS

LIST OF TABLES

LIST OF FIGURES

CHAPTER

1

INDTRODUCTION

In 1951, development of the world's first power producing fast breeder reactor - the Experimental Breeder Reactor (EBR-I) - left a historic landmark in the nuclear technology timeline [1]. Since then, fast reactors research has gained tremendous momentum around the world with renewed interest in development of Generation-IV type nuclear reactors. In a collaborative effort led by Generation-IV International Forum (GIF) aimed towards meeting the rapidly growing energy needs of the world, six new advanced reactor designs were selected [2]. These reactors systems included the Very High Temperature Reactor (VHTR), Gas-cooled Fast Reactor (GFR), Sodium-cooled Fast Reactor (SFR), Lead-cooled Fast Reactor (LFR), Molten Salt Reactor (MSR), and Supercritical Water-cooled Reactor (SCWR) [2]. Amongst these, LFRs emerged as one of the most promising, proliferation resistant, and sustainable reactor concepts offering safety and economic advantages over other fast reactor technologies [3].

Enhanced safety features of LFRs such as relatively inert coolant, retention of hazardous radionuclides including iodine and cesium in coolant, and high boiling point of lead at 1743 ^{o}C make it an optimal coolant choice for reactors with Heavy Liquid Metal Coolant (HLMC) [2, 3].

Lack of vigorous exothermic reaction between the coolant and air or water, favorable heat transfer, and excellent neutronic properties provide an opportunity for an open fuel lattice without compromising core pressure and neutron efficiency [3]. The compact vessel design from absence of an intermediate cooling circuit further accentuates the economic competitiveness of LFRs.

However, there is a significant lack in plant operational history of HLMC type reactors, compared to conventional Light Water Reactor (LWR) designs. As such, regulatory acceptance of LFRs relies on the quality and accuracy of reactor safety analysis. Safety parameters determined using modern codes have a direct impact from nuclear data and other uncertainties. Evaluation of these uncertainties will lead to a better understanding of their impact on reactor core design and identification of the design safety limits.

This scope of this work is development of a methodology for quantification of uncertainties of LFRs for safety analysis. This is accomplished by following a systematic approach, as outlined in Figure 1, where the first step is quantification of uncertainties on lattice level of modelling using best-estimate plus uncertainty methods. This is extended to whole core level to establish uncertainty bounds for selected reactivity feedback parameters. Top contributors of uncertainty are identified at various core modelling levels. Although different sources of uncertainties can impact core safety, the current emphasis is placed in quantification of nuclear data uncertainties originating from cross-section libraries. Figure 2 outlines the methods and tools used at various steps of this project as detailed in the next few chapters.

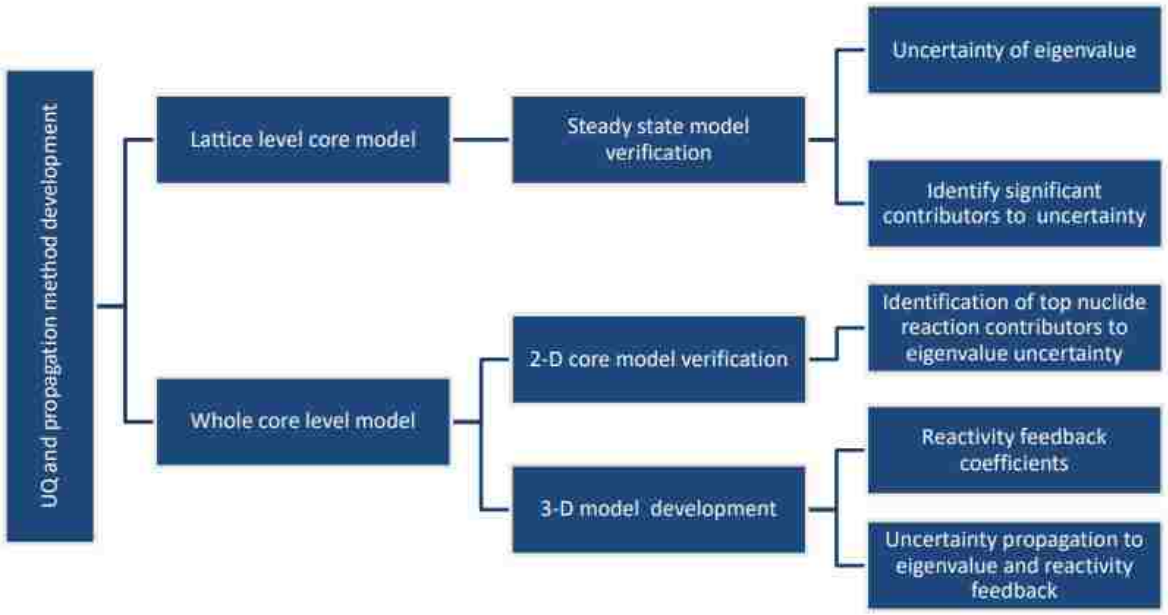

Figure 1: Plan of work overview

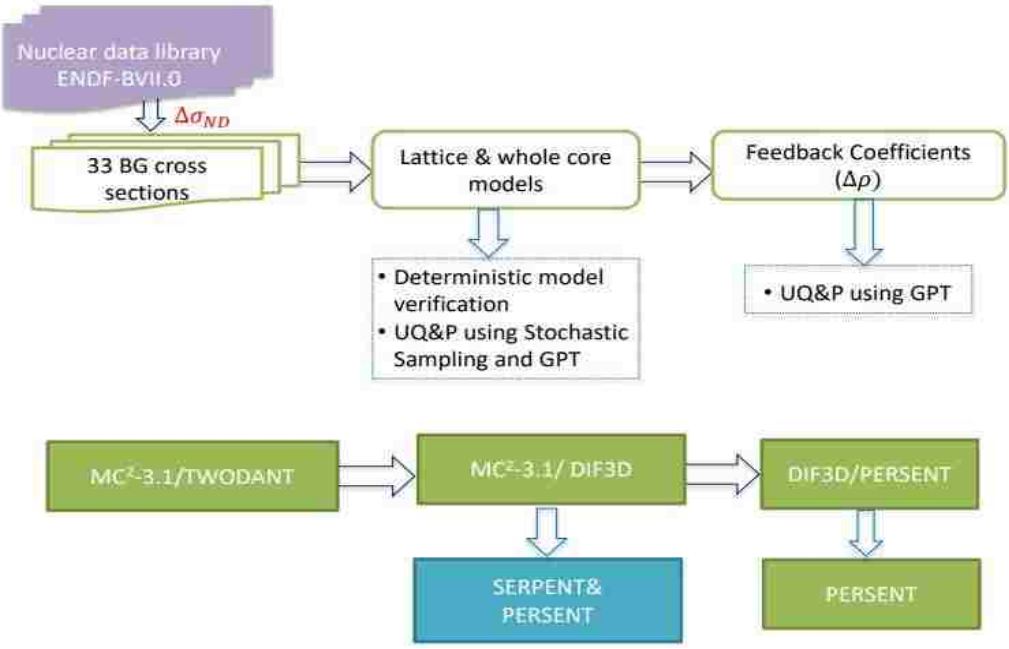

Figure 2: Overview of methodology and computational tools

In addition to above, an LFR reactor system is developed here to set up framework for propagation of such uncertainties through a system and assess their impact on safety parameters like fuel and clad temperatures.

This thesis is structured into various sections describing the approach and necessary background information. Chapter 1 outlines the necessary background information to understand the motivation for this research and form a plan of work. Chapter 2 gives the core description, specifications and provides an overview of the modelling tools for the chosen LFR design. Cross-sections generation methodology is explained in Chapter 3. Chapter 4 aims to establish a foundation for Sensitivity Analysis (SA) and Uncertainty Quantification (UQ). The results from initial implementation of UQ methodology for propagation of uncertainties are provided in Chapter 5. The final chapter proposes a research plan for further development of this research. The work completed in this thesis is the initial step towards propagation of nuclear uncertainties through Lead-cooled fast reactor system.

CHAPTER

2

CORE DESING, SPECIFICATION, AND MODELLING

2.1 Demonstration Lead-cooled Fast Reactor Design

The Demonstration Lead-Cooled Fast Reactor (DLFR) was originally conceptualized by Westinghouse Electric Company (WEC) as an option for the advanced demonstration and test reactor study conducted by the Department of Energy (DOE). WEC developed the DLFR in collaboration with Argonne National Lab (ANL) and the Italian National Agency for New Technologies, Energy and Sustainable Economic Development (ENEA) with the objective of providing an insight into feasibility and basic performance of the LFR technology.

The motivation for selecting this specific reactor design for this research is based on DLFRs capabilities of providing a commercially viable reactor technology. It features a compact, pool-type design rated at 500 MW_{th}, which is suitable for modular construction and enhanced economic benefits. In addition to being one of the first commercial LFR demonstration designs in the past decade in United States, the DLFR design was optimized for feasible inspection, maintenance and replacement of the primary system and components [4].

The pool type layout of the primary system with reactor coolant pumps (RCPs) incorporated into the steam generator (SG) is provided in Figure 3. As explained in reference [4], designs of the SGs for DLFR were adopted from the ELSY reactor design. RCPs draw the coolant from hot pot pool near the core to the SGs which are located above the core. Cold lead flows back through the downcomers entering the core from the bottom. The main reactor vessel contains all primary components immersed in liquid lead. All cladding and other in-core components are made of authentic 15-15Ti stainless steel, which is qualified for use in a nuclear reactor with oxide fuel. In addition, the entire main vessel, comprising of the core barrel and outer wall, is made of stainless steel class AISI 316L. Table 1 summarizes relevant design specifications for core modelling complimenting the information provided in this section.

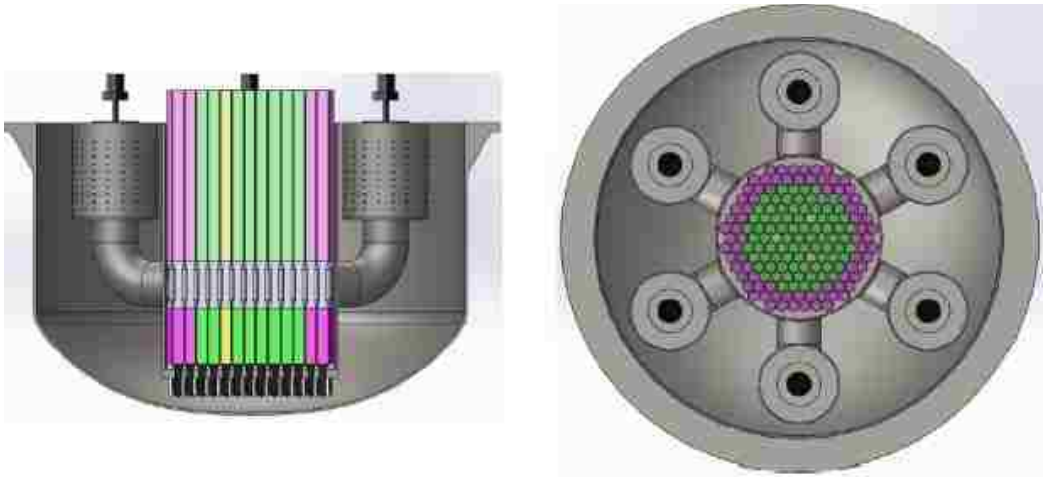

Figure 3: Conceptual Vertical (left) and horizontal (right) cross sections of the DLFR primary system showing core and SG layouts [4]

Table 1: DLFR Core Specifications

Parameter Description	Value	Unit
Reactor thermal power	500	MW
Core-average T_{out}	510	^{o}C
Core T_{in}	390	^{o}C
Fuel	UO_2	-
Maximum ^{235}U enrichment	20	%
Fuel Cycle Length	12	Months
Average burmup	100	MWd/kg_{HM}
Number of inner core assemblies	34	-
Number of outer core assemblies	42	-
Fuel pins per assembly	432	-
Fuel assembly pitch	30.4	cm
Fuel pin pitch	1.36	cm

2.1.1 Reactor Core

DLFR reactor core operates on a 12 month fuel cycle, using uranium oxide (UO_2) as fuel however the subsequent reloads can utilize uranium nitride (UN) fuel as well. The primary coolant is chosen to be Russian "C1" standard nuclear grade liquid lead for coolant. The core consists of the 163 hexagonal sub-assemblies arranged in a triangular lattice to form a pseudo-cylinder as shown in Figure 5. There are 82 fuel assemblies separated into inner and outer core, surrounded by 78 reflector/shield assemblies.

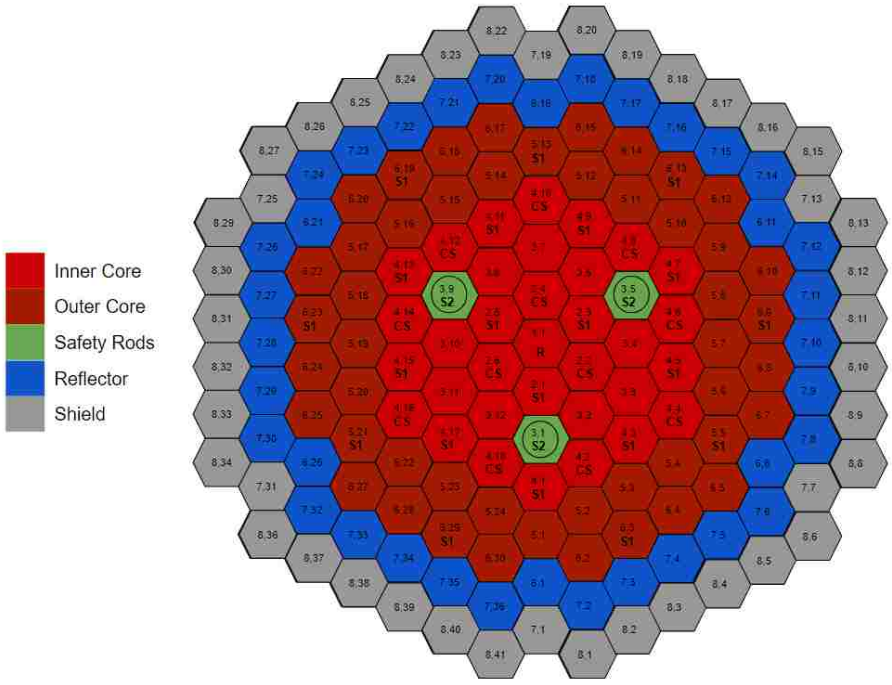

Figure 4: Radial layout of the DLFR reactor core. S1, S2, CS and RS represent the safety system 1, safety system 2, control system and regulation system employed within the reactor core. The assemblies are identified with coordinates representing ring and assembly numbers.

Each fuel sub-assembly can accommodate 469 positions arranged in a triangular lattice where the central 37 positions are replaced by beam tube, as shown in Figure 5. The central beam tube is a hollow hexagonal cylinder that can be used for hosting instrumentation rods, controls rods or irradiation experiments. Remaining 432 positions in the subassembly are occupied by fuel pins containing stacks of sintered enriched uranium pellets. More information on core design and specifications in reference [4].

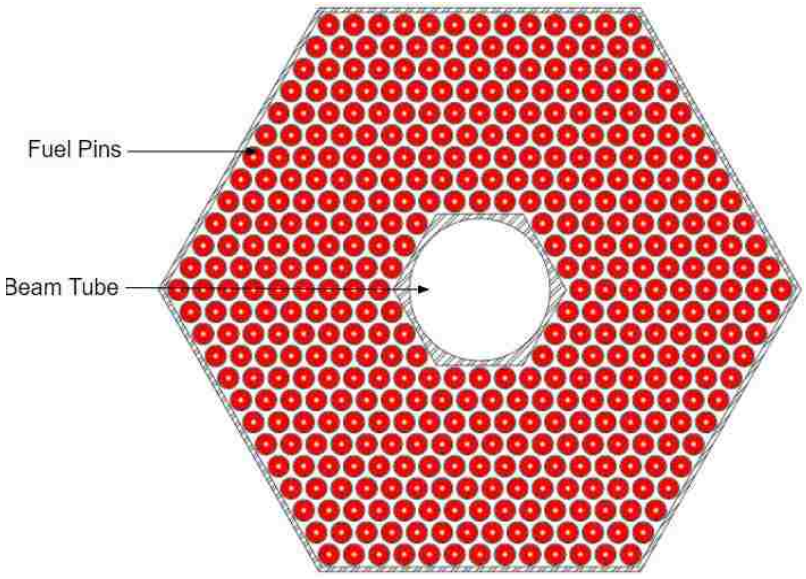

Figure 5: DLFR fuel subassembly radial layout [4]

2.1.2 Control Systems

DLFR is controlled using a unique set of control rods called finger absorber rods (FARs) separated into four banks – safety system 1 (S1), safety system 2 (S2), regulation system (RS), and control system (CS), also shown in Figure 4. Each bundle of these absorber pins contain up to 90% ^{10}B-enriched which can be inserted from top (S1 and RS) or bottom (S2 and CS) of the core in the central beam tube of the subassembly (Figure 6). The CS rods are envisioned to have yttrium stabilized zirconia (YSZ) as reflector material stacked atop the boron carbide such that when the rods are withdrawn, reflector part of the FARs is aside active core as shown in Figure 6. CS rods have the highest worth and are extracted alternatingly with RS rods from the core to achieve criticality at startup. Once CS is fully extracted, any small amount of excess positive reactivity can be fine-tuned by re-inserting RS into the core. The S1 safety system is reserved atop the core by reactor protector system in case of failure of the CS system. S2 consists of three massive safety rods designated for SCRAM [4]. The total rod worth of each system can be found in Table 2.

Table 2: Total rod worth in each control bank

Bank	Total Rod Worth (pcm)
RS	300
CS	3700
S1	1700
S2	1700

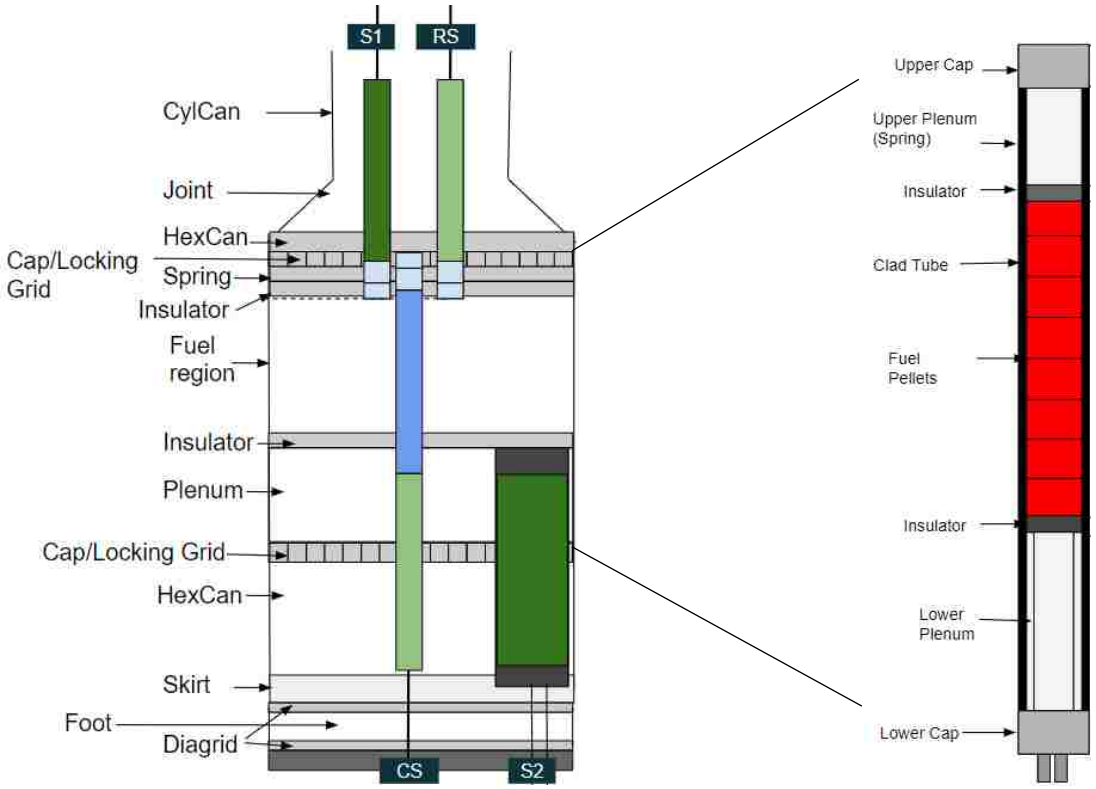

Figure 6: Simplified axial layout of the fuel assembly (left) and the fuel pin (right) as modelled

2.2 Core Modelling

The reactor core is primarily modeled using ANL fast reactor analysis 'Argonne Reactor Computation' (ARC) code suite [5]. It comprises of multiple tools for handling different parts of fast reactor core modelling and analysis such as cross-section generation, modelling, perturbation calculation, core depletion etc. Lattice level modelling code MCC-3.1 in ARC performs transport

calculations on homogenized 0D mixture geometry [6]. However, bearing in mind the complexity of the DLFR fuel assembly with presence of FARs in the central beam tube, Monte Carlo code SERPENT-2.0 is considered for lattice calculations instead [7]. The purpose of using Monte Carlo code at this stage is to truly capture the heterogeneity effects of DLFR fuel assembly and quantify the difference between the explicit model in SERPENT and homogeneous model in MCC-3.1. The reference results were obtained from transport code ERANOS using ECCO [8]. This section provides further information on these codes, and any modelling variations for properly adapting the available tools.

The DLFR models in SERPENT-2.0, shown in Figure 7, uses cross-sections generated from nuclear data library ENDF/B-VII.0.

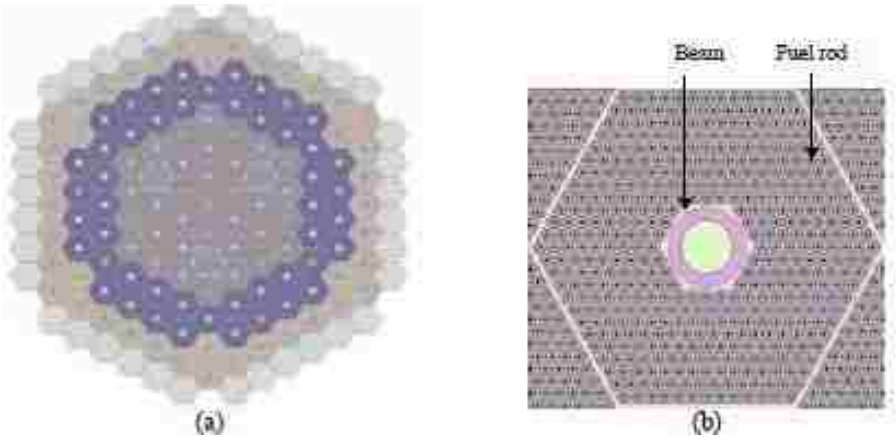

Figure 7: DLFR core (a) and fuel assembly (b) models in SERPENT-2.0

The 3D core DLFR model, (Figures 4) is developed in ARC suite. Within ARC, cross-sections are generated using MCC-3.1 coupled with 2D S_n transport solver code TWODANT [6, 9]. These cross-sections are used as inputs in computational code DIF3D for flux calculations using variational nodal transport solver (VARIANT) [10]. The angular flux solution and scattering approximation are expanded to the 3rd order. The core is assumed at all rods out condition and the

safety rods (S2) withdrawn below core (Figure 6). An axial temperature gradient, provided by ENEA, is maintained for all core components above, below and at core level during the reactor core model setup [4]. Consequently, temperature dilatation effects on all structural geometry and densities was considered for correct neutronic simulation at operating temperatures. All dimensions and densities were carefully adjusted by factors governed by their respective coefficient of linear thermal expansion described by $\alpha_T = \frac{1}{L}\left(\frac{dL}{dT}\right)$. Specifics on thermal expansions of fuel, coolant and all other materials can be found in references [11] and [12].

CHAPTER

3

CROSS-SECTION GENERATION METHODS

In core calculations, the first step is to generate multi-group cross-sections. This calculation is performed using lattice codes which solves the multi-group Boltzmann transport equation given as

$$\frac{1}{v}\frac{\delta\phi}{\delta t} + \hat{\Omega}\cdot\nabla\phi + \Sigma_t(r,E)\phi\left(r,E,\hat{\Omega},t\right) = \int_{4\pi} d\hat{\Omega}' \int_0^{\infty} dE'\Sigma_S\left(E'\to E,\hat{\Omega}'\to\hat{\Omega}\right)\phi\left(r,E',\hat{\Omega},t\right) + s\left(r,E,\hat{\Omega},t\right) \quad (1)$$

where,

(a) $\frac{1}{v}\frac{\delta\phi}{\delta t} =$ Rate of change in neutron population

(b) $\hat{\Omega}\cdot\nabla n =$ Leakage

(c) $\Sigma_t(r,E)n\left(r,E,\hat{\Omega},t\right) =$Loss due to collision

(d) $\int_{4\pi} d\hat{\Omega}' \int_0^{\infty} dE'\Sigma_S\left(E'\to E,\hat{\Omega}'\to\hat{\Omega}\right)n\left(r,E',\hat{\Omega},t\right) =$ Gain due to in scattering

(e) $s\left(r,E,\hat{\Omega},t\right) =$Rate of source of neutrons

Using flux solutions from the transport equation, condensed multi-group, and self-shielded cross-sections are obtained using nuclear data files. It is important to preserve reaction rates when these condensing cross-sections. In MCC-3.1, P_1 multi-group transport equation is solved for generation the multi-group neutron cross-sections using either homogeneous, 1D heterogeneous slab or cylinder geometry. The cross-sections in ultrafine group (~2000) are self-shielded by numerical integration of point wise cross-sections based on narrow resonance approximation [6].

Conventional method for cross-section generation in ARC using the multi-group cross-section generation code MCC-3.1 for obtaining self-shielded cross-sections is shown in Figure 8. First, the core is represented with a 0D mixture geometry for each assembly. MCC-3.1 calculates condensed region wise self-shielded 230 ultrafine group (UFG) cross-sections using 2082 groups master isotopic library and provides them to TWODANT [6]. TWODANT performs transport calculations on an equivalent R-Z model of the core to obtain region-wise flux solutions with 230 UFG cross-sections [9]. Finally, MCC-3.1 generates region-wise 33 broad group (BG) condensed cross-sections using the UFG flux solutions obtained in the previous step [6].

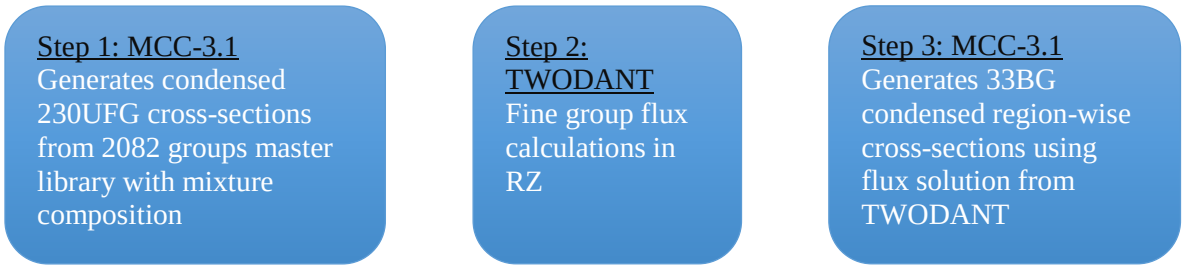

Figure 8: Conventional cross-section generation methodology in ARC (UFG and BG refer to Ultra Fine Group and Broad Group, respectively)

However, one of the main challenges of modelling DLFR using ARC is during cross-section generation process due to subassembly geometry. The DLFR subassemblies have radial

heterogeneity within the subassembly due to presence of absorber material in the central beam tube (figure 5). The conventional cross-section generation method in MCC-3.1 uses complicates the process of generating properly self-shielded cross-sections considering the 0D homogenized geometry utilized in step 1 (Figure 8). Intermediate steps were necessary to obtain properly self-shielded cross-sections reflecting the true material distribution the fuel assembly. This involved improved implementation of the conventional cross-section generation methodology. The primary purpose of this method is the proper treatment of the self-shielding effects due to absorber material in the center of fuel assemblies. Figure 9 provides a schematic understanding of the improved cross-section generation methodology.

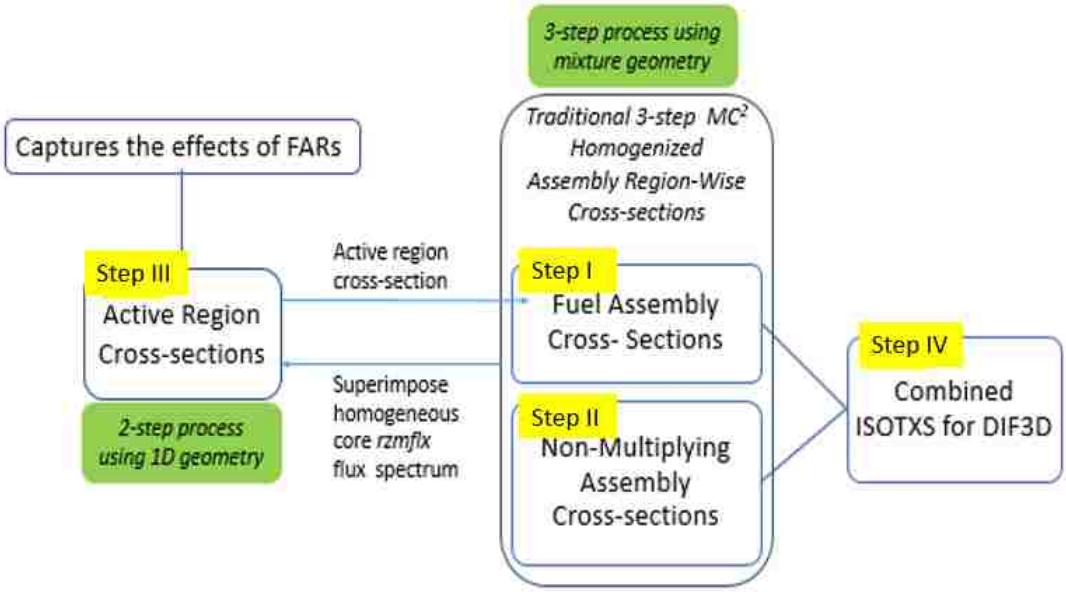

Figure 9: Schematic representation of the improved cross-section generation methodology

I. Fuel assembly cross-sections

i. A DLFR fuel subassembly (Figure 6) is represented with 0D homogenized axial regions in mixture geometry.

ii. Similar to step 2 in Figure 8, the fuel subassembly is represented with an equivalent RZ model in TWODANT to generate region-wise flux solutions in axial direction.

iii. Condensed 33 BG axial leakage corrected cross-sections are generated by MCC-3.1 using flux spectrum from step ii for one fuel subassembly type. Steps i-iii are then repeated for each fuel subassembly type. In DFLR, there are six different fuel subassembly types between inner and outer core, i.e. inner core assembly without FAR, inner core assemblies with RS, S1, and CS type FARs, outer core assembly without FAR, outer core assemblies with S1 type FARs. Total of six separate cross-section calculations are performed at this stage.

II. Non-multiplying assembly cross sections

i. Cross-sections for non-multiplying assemblies (shield, reflectors and S2 safety system) are generated using the traditional process outlined in Figure 8. The core is represented using homogenized mixture geometry for different subassemblies. The region-wise flux solutions from TWODANT are saved in an *rzmflx* file.

III. Fuel assembly active region cross sections

i. An additional step is included here for incorporating radial leakage in the fuel cross-sections from step iii. A separate set of calculation is performed for the active core region of the fuel subassemblies utilizing the 1D heterogeneous cell treatment capabilities of MCC-3.1 [13]. In this method, 1D cylindrical geometry option of MCC-3.1 is adapted by superimposing *rzmflx* flux spectrum from step iv to the 1D cell

transport solutions of step v. This approach simultaneously allows taking into account the heterogeneity effects in the fuel region and leakage effect between regions in core. Figure 10b shows the 1D fuel assembly model where the beam tube and fuel rings in Figure 10a, correspond with equivalent cylindrical rings 1, 2, etc. Each cylinder is subdivided into 1D sub-cylinders separating the materials contained within the original cylinder. More details on this methodology can be found in reference [13].

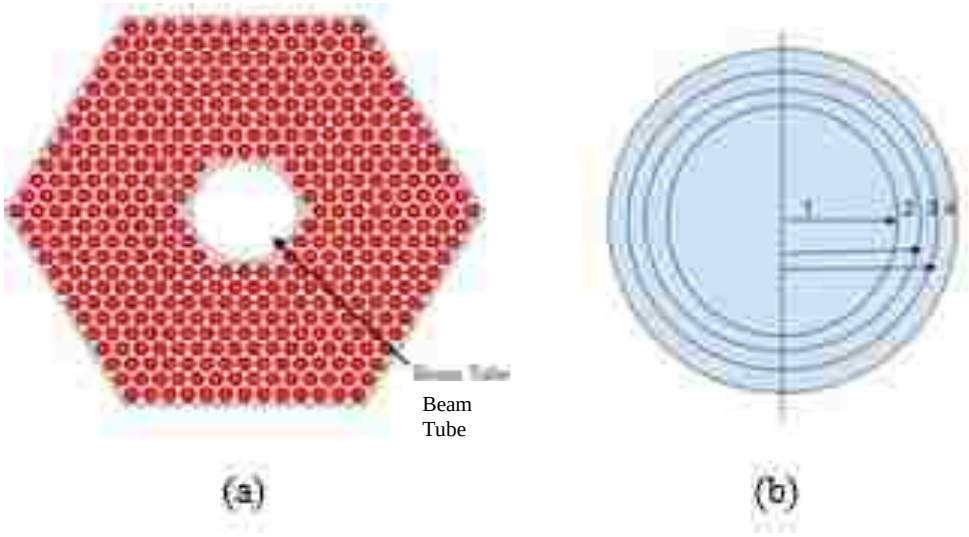

Figure 10: 1D cylinder representation of the fuel assembly

IV. Merged cross-sections

i. Different region cross-sections from all subassemblies are merged into one ISOTXS format file for all other computations.

CHAPTER

4

UNCERTAINTY QUANTIFICATION AND PROPAGATION

Quantifying the uncertainties in a new system design is crucial to understanding its safety capabilities during design based events and accidents. Throughout the core design process, many sources of uncertainties such as those from fuel modelling, thermal hydraulics, etc. can be introduced at different stages of modelling, as seen in Figure 11. Proper handling and propagation of uncertainties is therefore necessary to establish confidence bounds on core safety and performance parameters. Currently, only nuclear data uncertainties are being considered through the system. This section provides an overview of the uncertainty quantification methodology and the systematic approach followed for propagation of these uncertainties through the reactor system.

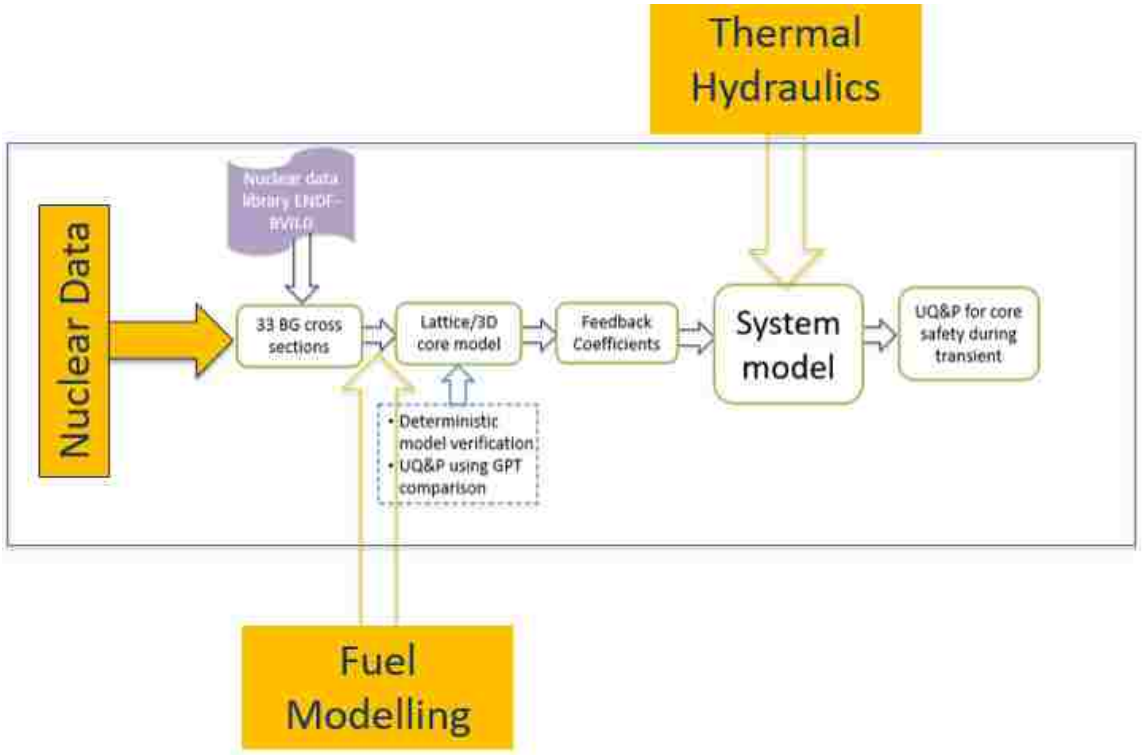

Figure 11: Sources of uncertainties in a reactor and system design

4.1 Sensitivity and Uncertainty Analysis for Steady State

To compute the influence of uncertainties on the output for a given model UQ&P of input uncertainties is needed. In a large or complex model, with multiple perturbed system equations for each input variation, the propagation of uncertainty via sampling-based methods is not feasible. One of the alternatives is a perturbation method which is based on truncating the Taylor expansion of a response parameter [16]. Consider a set of random variables $Q = [Q_1, Q_2, \dots, Q_p]$. The first order linear expansion for the model response $f(Q)$ is

$$f(Q) = \bar{y} + \sum_{i=1}^{p} s_i \delta Q_i \tag{2}$$

where $\bar{y} = f(\bar{q})$ and $s_i = \frac{\partial f}{\partial Q_i}(\bar{q})$ defines the sensitivity of the response function at $\bar{q}$.

Covariance of Q_i with Q_j is expressed as

$$cov(Q_i, Q_j) = \int_{\mathbb{R}} (q_i - \bar{q_i})(q_j - \bar{q_j})\rho_Q(q)dq \quad (3)$$

Where $\rho_Q(q)$ is the probability density function of Q

and the expectation of Q can be defined as $\mathbb{E}(Q) = \bar{q_i}$.

$$\mathbb{E}[f(Q)] = \bar{y}\int_{\mathbb{R}^P} \rho_Q(q)dq + \sum_{i=1}^{p} s_i \int_{\mathbb{R}^p} (q_i - \bar{q_i})\rho_Q(q)dq = \bar{y} \quad (4)$$

Evaluating the integrals in the above equation where the first integral is unity and second is zero, variance of $f(Q)$ is

$$var[f(Q)] = \mathbb{E}[(f(Q) - \bar{y})^2] \quad (5)$$

Using Eq (2),

$$var[f(Q)] = \int (\sum_{i=1}^{p} s_i \delta Q_i)^2 \rho_Q(q)dq = \sum_{i=1}^{p} s_i^2 var(Q_i) + \sum_{i=1}^{p}\sum_{\substack{j=1 \\ j\neq i}}^{p} s_i s_j cov(Q_i, Q_j) \quad (6)$$

This can be rewritten in matrix form, also known as the "sandwich rule", as

$$var[f(Q)] = S^T D S \quad (7)$$

where *D* is a covariance matrix for *Q* and *S* the sensitivity matrix. Determining the sensitivity coefficients of the response parameter using computational tools is the key factor to this approach [16].

In the current study, the Best Estimate Plus Uncertainty (BEPU) approach was applied to the DLFR core to evaluate the impact of uncertainties on the nuclear data. The generalized perturbation

theory (GPT) based method was used for building a deterministic model. GPT uses deterministic sensitivity and uncertainty methods to compute sensitivity coefficient S_ρ to relate relative change of an integral core parameter (such as multiplication factor) to the relative change in multi-group nuclear data, σ_g. Once the sensitivity matrix (S_i) associated with each integral parameter is obtained, the total contribution of uncertainties attributed to these coefficients can be determined using correlations and covariance matrices.

For a given core parameter $\Delta\rho_i$, the sensitivity coefficient S_ρ is defined as:

$$S_R = \begin{bmatrix} S_1 \\ \vdots \\ S_i \\ \vdots \\ S_N \end{bmatrix} \qquad for\ 1 \le i \le N \tag{8}$$

where $N =$ Nuclide-reaction number $\times$ energy groups. For example, for ^{235}U fission reaction for 33 energy groups, $N = 1 \times 33$. Each sensitivity coefficient is

$$S_{j,x,g} = \frac{\partial\rho/\rho}{\partial\sigma_{j,x,g}/\sigma_{j,x,g}} = \frac{\partial\rho}{\partial\sigma_{j,x,g}}\frac{\sigma_{j,x,g}}{\rho} \tag{9}$$

where *j*, *x* and *g* represent the isotope, the cross-section type, and the energy group, respectively.

Using the nuclear data uncertainties associated with the ENDF/B-VII.0 libraries provided in 33-energy macro-groups covariance library, COMMARA-2.0, defined as [17]:

$$D = \left(D_{x,j}\right) = \begin{bmatrix} D_{11} & D_{12} & \cdots & \cdots & D_{1N} \\ D_{21} & \cdots & & & \\ \vdots & & D_{jj} & & \\ \vdots & & & \cdots & \\ D_{N1} & & & & D_{NN} \end{bmatrix} \quad for\ N = 33\ energy\ groups_{x,j} \qquad (10)$$

Uncertainty I_i^{2}[1] for reactivity coefficient ρ_i can be obtained using the "sandwich rule" discussed above:

$$I_i^2 = S_i^T D S_i \qquad (11)$$

Using the above describe GPT methodology, impact of nuclear data uncertainty is studied on lattice level as well as used to quantify uncertainty in reactivity feedback coefficients. The focus of this study is placed on five different feedback coefficients including Doppler coefficient, radial expansion coefficient and fuel/coolant/structure density worth. The feedback coefficient α is obtained as a change in reactivity between base and perturbed core states caused by a change in core parameters (temperature/density/pitch). The sensitivity $S_{\alpha,\sigma}$ of a given feedback coefficient α to perturbations in nuclear data can be calculated from sensitivity of reactivity change ρ by $S_{\rho,\sigma}^{j} = \frac{\partial \rho_j}{\partial \sigma_{i,x,g}} \frac{\partial \sigma_{i,x,g}}{\rho_j}$ for base (j=1) and perturbed (j=2) cases. The indices *i*, *x* and *g* represent the isotope, the cross-section type and the energy group respectively. For Doppler coefficient, base case obtains the sensitivity of reactivity ($S_{\rho,\sigma}^{1}$) to nuclear data perturbations at nominal temperature. Similarly, perturbed case provides sensitivities ($S_{\rho,\sigma}^{2}$) at Doppler temperature. Then, Eq. 1 is used to obtain sensitivity of feedback coefficient $S_{\alpha,\sigma}$ by combining $S_{\rho,\sigma}^{1}$ and $S_{\rho,\sigma}^{2}$ using the reactivity change ($\Delta\rho = \frac{1}{k^1} - \frac{1}{k^2}$) from the base to the perturbed case [21]:

[1] It should be noted that, mathematically I_i^2 represents uncertainty contribution to parameter *R* due to the respective cross-section.

$$S_{\alpha,\sigma} = \frac{\frac{S^2_{\rho_2,\sigma}}{k^2} - \frac{S^1_{\rho_1,\sigma}}{k^1}}{\Delta\rho} \quad (12)$$

The total uncertainty I_n^2 of α can now be described using equation 11.

Sensitivity matrix of the eigenvalue and reactivity feedback coefficients is obtained using ANL perturbation theory based code PERSENT. PERSENT employs the adjoint-based sensitivity analysis to generate the sensitivity coefficients. In this methodology, the sensitivity functions are evaluated using adjoint variables without solving perturbed system equations for each input parameter change. PERSENT uses variational methods for the adjoint-based sensitivity analysis where the solution of the corresponding adjoint transport equation is used to compute changes in eigenvalue based on perturbations in the cross section. [18, 19].

The GPT methodology applied on ARC results to compute total contribution on uncertainties is verified using the GPT capabilities implemented within SERPENT. The sensitivity coefficients in SERPENT are generated using a collision-history based approach explained further in reference [20].

4.2 Variance-Covariance Data

The covariance matrix used in this study - COMMARA-2.0 - was released by Los Alamos National Lab (LANL) and Brookhaven National Lab (BNL). It contains information on neutron cross-section covariance for various materials. The covariance are given in 33 energy groups for energy range from 19.6 MeV down to 10-5 eV. They are built from the ENDF/B-VII.0-based covariance library by processing through NJOY with 1/E flux [17].

CHAPTER

5

RESULTS AND DISCUSSION

The preliminary nature of this work makes it necessary to quantify the extent to which the results can be trusted. In absence of experimental data, verification methods such as code-to-code comparison eliminate errors and ensure that the model behaves as the user intended. Therefore, lattice models developed lattice models developed here using deterministic ARC codes are verified against Monte Carlo code SERPENT for various core performance parameters including criticality, power, and flux profiles.

This section first presents the lattice level criticality results from base case models developed in MCC-3.1 which are verified with an explicit model in SERPENT. This quantifies the difference between the SERPENT and ARC in terms of reactivity. Upon establishing an acceptable level of difference at assembly level, a nominal case is developed for whole core model verification as explained in the following sections.

5.1 Lattice Model Verification

Initial results obtained from SERPENT and MCC-3.1 using models described in Chapter 2 are summarized in Table 3, where BOC/EOC refer to Beginning of Life, Beginning of Cycle, End of

Cycle, and End of Life in core composition, respectively. Neutron population in SERPENT is set to 100000 with 500 active and 50 inactive cycles. The models are at all rods out core condition.

Table 3: Eigenvalue results for nominal case from SERPENT and DIF3D

	SERPENT	MC^2-3.1	Δpcm	% δk/k
Outer Core	k_∞			
BOC	1.28194±0.00014	1.28121	44.4	-0.05
EOC	1.25681±0.00015	1.25813	-83.5	0.10
	SERPENT	DIF3D		
2D Core	k_∞			
BOC	1.17683±0.00018	1.1688	583.8	0.66
EOC	1.15126±0.00017	1.1437	574.2	0.91

Eigenvalues at assembly level show less than 100 pcm difference between the fully heterogeneous in SERPENT model and the homogenized assembly model in MCC-3.1. However, this difference at 583.8 pcm is significantly larger on 2D core level. Comparing the two models, the source of the observed differences is attributed to the two different methods of cross-section generation between SEPRENT and MCC-3.1 along with the explicit model used in SERPENT.

Further comparing the power distributions from the two codes for the 2D core model in Figure 12, an acceptable level of difference in the power distribution for 1/3rd core is observed. The relative present difference is less than 10% for inner assemblies. The assemblies showing larger differences of 11.6%, 13.4%, 14.8%, and 16.1% are in the outer core near reflectors which can explain the large difference due to flux distortions in that region.

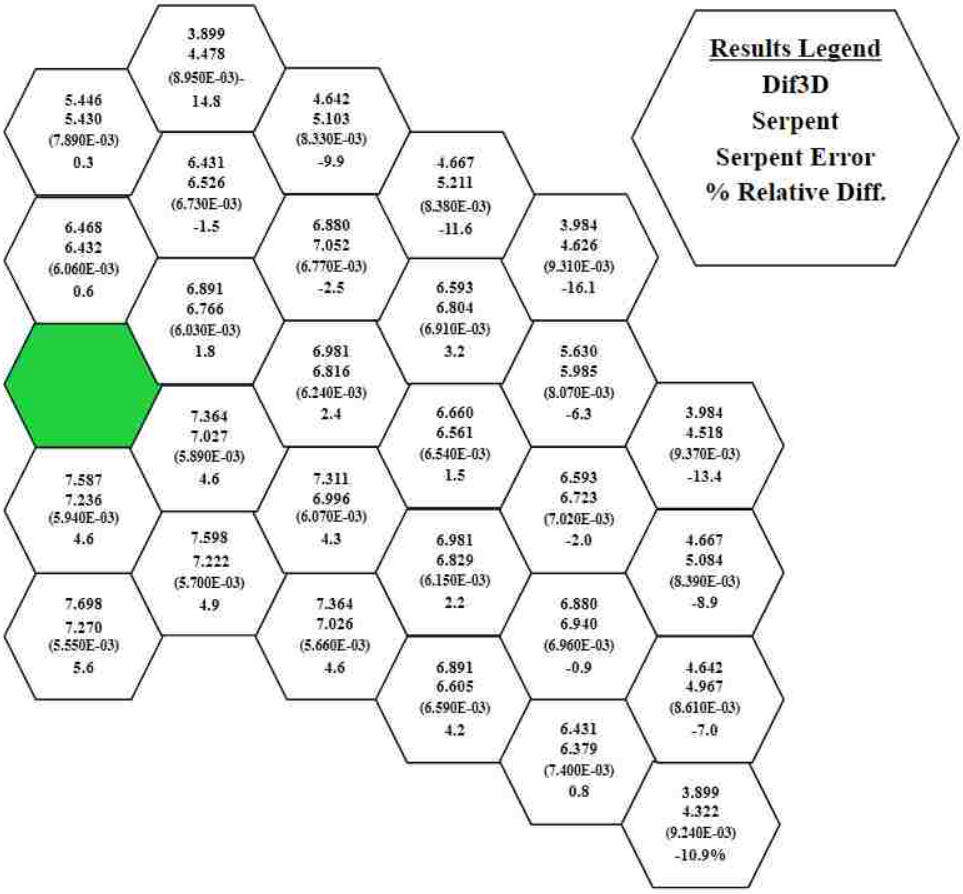

Figure 12: 2D Assembly wise power distribution for 1/3rd core

Additionally, Figure 13 provides comparison of the flux distribution in the central fuel assembly from SERPENT and DIF3D. Although a good overlap is seen between the two results, the difference in peak values is noticeable based on how the energy bins are tallied. The Monte Carlo relative statistical error from SERPENT for all flux data is to order of 10^{-3}. In DIF3D, ANL 33 group energy structure is used, whereas the 33 group structure of ECCO is used in SERPENT. Both energy group structures can be found in Appendix C.

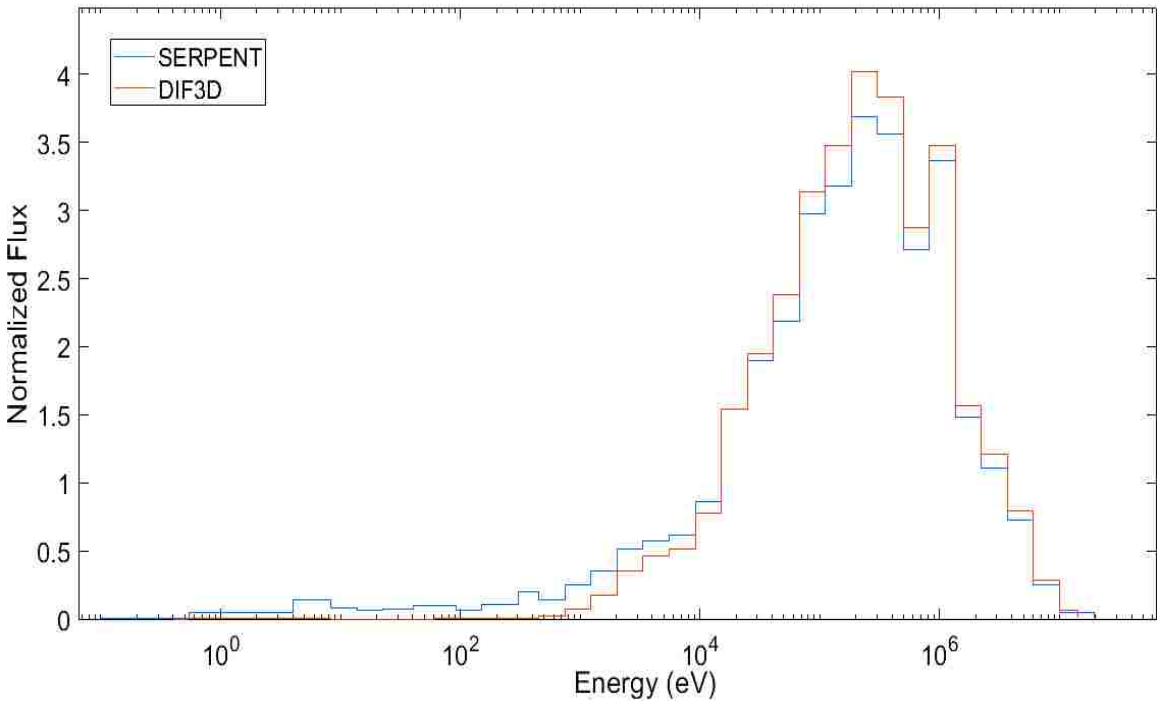

Figure 13: Flux distribution for central assembly (1, 1)

5.2 Whole Core Level

A full core steady state model is developed in DIF3D for the purpose of this work. However, as explained in Chapter 3, an improved method for cross-section generation was implemented considering the axial and radial heterogeneity of the DLFR core. To demonstrate the improvements from cross-section generation methodology and understand reactivity feedback responses to variations in core temperature (Chapter 4), 3-D full core is modelled in DIF3D.

Based on methodology explained in Chapter 3, two sets of cross-sections were generated using methods outlined Figures 8 and 9 for the same core model in DIF3D. Respective eigenvalues were compared at BOC to note a 950 pcm difference between the two. The conventional method provides a lower eigenvalue due to homogenization of fuel and absorber within the assembly. Therefore, considering the importance of correctly self-shielded cross-sections and the observed

differences, the improved cross-section generation approach is adapted for assessing all core performance parameters. Using the new cross-section generation method, a k_{eff} of 1.03321 is obtained at BOC. Future work is underway to verify the improved cross-section generation methodology as explained in Chapter 5.

This model is then used to generate selected five reactivity feedback coefficients which are summarized in Table 4 below.

Table 4: Reactivity feedback coefficients for DLFR

Feedback Parameter	**Perturbation Type**	**Degree of Variation**	**Reactivity [pcm]**	**Coefficient (pcm/K)**
Doppler	Fuel temperature (Nominal at 926 ^{o}C)	+500 ^{o}C	-713.51	-0.9240
Radial Expansion	Core pitch	+2.5%	-851.31	-0.8314
Structure Density	15-15Ti SS Density in active region	-5%	116.53	0.1551
Coolant Density	Lead Density in active region	-5%	-70.51	-0.1720
Fuel Density	Fuel Density	-5%	-1423.98	-2.1450

Large negative reactivity is expected for Doppler coefficient, as increase in fuel temperature will lead to Doppler broadening of resonances and increased neutron absorption. Due to energy self-

shielding effects a depression in flux in vicinity of resonance peaks will also contribute to the negative reactivity. In radial expansion coefficient, core pitch is expanded while preserving mass of fuel and structure. Increase in coolant volume inside the core with increased moderation of neutrons leads to addition of net negative reactivity. Similarly, when fuel density expands, the fissile nuclide concentration is also reduced adding negative reactivity to the core. For coolant density expansion reactivity feedback, net negative reactivity is added based on the competing effects of positive reactivity from reduced amount of coolant per unit volume, negative reactivity from increased leakage, and positive reactivity from decreased neutron capture. The coolant reactivity feedback is design dependent. For structure density expansion coefficient, large positive reactivity is added. Positive reactivity is expected since decrease in clad density leads to decreased interaction between neutrons and steel.

5.3 Uncertainty Quantification

5.3.1 Lattice Level

On fuel assembly level, the sensitivity and uncertainty calculations were performed in SERPENT - where the assemblies were modelled heterogeneously. Figures 14-17 show the sensitivity and uncertainty profiles generated at BOC and EOC for inner core assembly (1, 1). Table 5 provides a comparison of the nuclear data uncertainty contribution break down from BOC to EOC for the same inner core assembly. Additionally, results for the equilibrium core composition are provided in Appendix D.

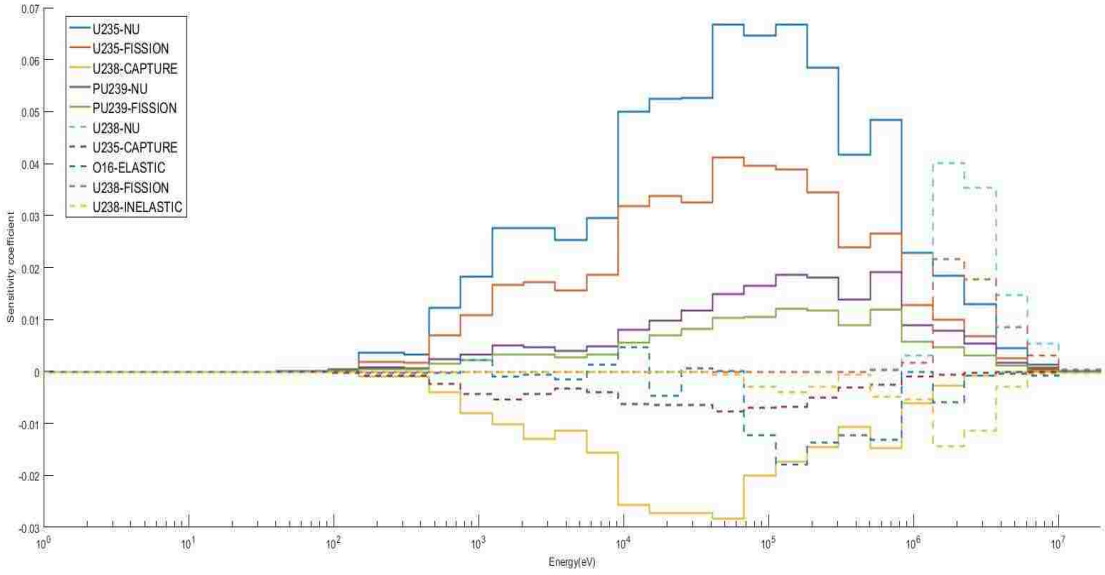

Figure 14: Sensitivity of inner core assembly (1, 1) k_{inf} at BOC

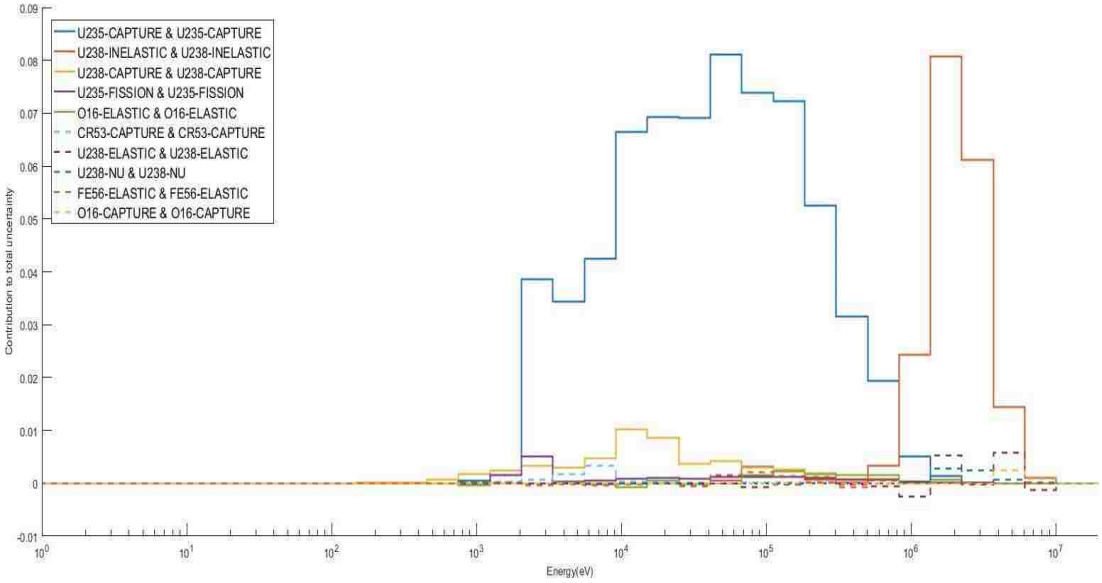

Figure 15: Uncertainty of inner core assembly (1, 1) k_{inf} at BOC

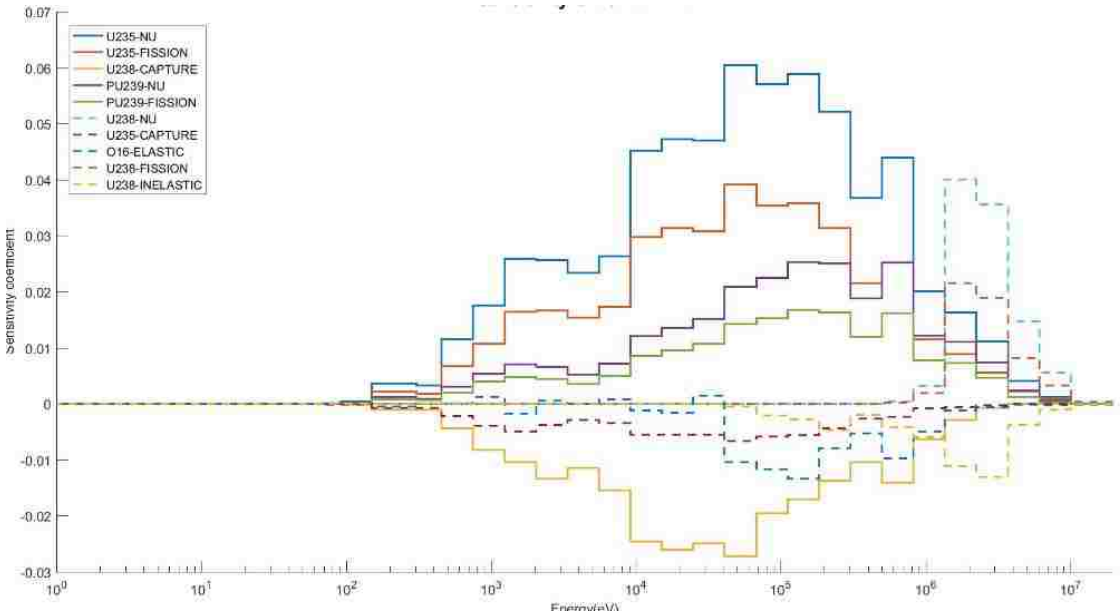

Figure 16: Sensitivity of inner core assembly (1, 1) k_{inf} at EOC

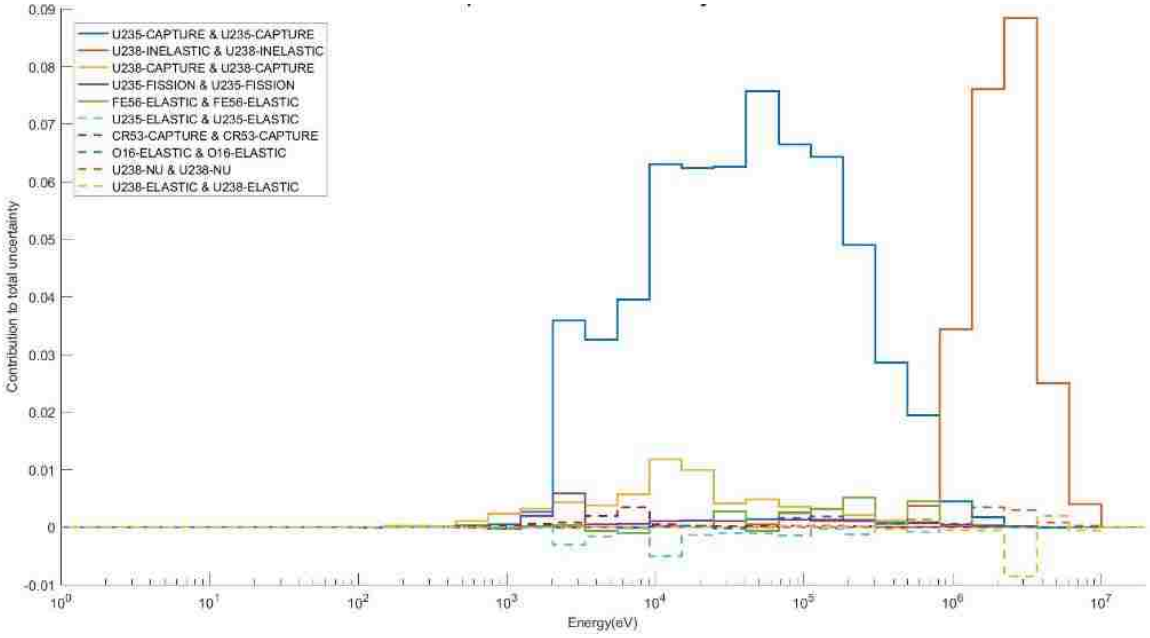

Figure 17: Uncertainty of inner core assembly (1, 1) k_{inf} at EOC

Table 5: Breakdown of uncertainty in k∞ for an inner assembly from SERPENT

Rank	Uncertainty Contribution (%)			
	Nuclide/nuclide reaction	**BOC**	**Nuclide/nuclide reaction**	**EOC**
1	^{235}U(n,γ)/ ^{235}U(n,γ)	65.8	^{235}U(n,γ)/ ^{235}U(n,γ)	60.9
2	^{238}U(n,n')/ ^{238}U(n,n')	19.1	^{238}U(n,n')/ ^{238}U(n,n')	23.8
3	^{238}U(n,γ)/ ^{238}U(n,γ)	5.11	^{238}U(n,γ)/ ^{238}U(n,γ)	6.3
4	^{235}U fission/ ^{235}U fission	1.74	^{235}U fission/ ^{235}U fission	1.72
5	^{16}O (n,n)/^{16}O (n,n)	0.09	^{56}Fe (n,n)/^{56}Fe (n,n)	1.52
Total contribution to k∞		**1.50**		**1.35**

Based on the sensitivity results, uncertainties for nuclide reaction pairs were computed using the "sandwich rule" described in Chapter 4. The largest contribution to uncertainty in k_{inf} comes from heavy metals - ^{235}U and ^{238}U. Both quantities have a decreasing trend as the core depletes however it is important to note that the uncertainty trend remains consistent. Positive sensitivity profiles implies a positive linear relationship between perturbations in the input and its effect on the output, whereas negative profiles show a non-linear relationship between the output and the input. For the negative profiles, as the input is increased, the output shows a decrease and vice versa.

Using the covariance matrix COMMARA 2.0, uncertainty calculations are performed to generate the uncertainty profiles. Correlations between different nuclides reaction pairs are used to

determine the contribution of uncertainty to the k_{inf}. The correlations show the statistical relationship between two nuclide reaction types. ^{235}U capture-^{235}U capture reaction pair has a strong positive correlation – as is also the case for ^{238}U -inelastic scattering pair. The multiplication factor is noticeably sensitive to perturbation in the ^{235}U fission and ^{235}U capture cross sections which lead to a large uncertainty contribution to the multiplication factor based on their positive correlation coefficients.

5.3.2 Uncertainty Quantification on 2D Core

On the core level, the sensitivity coefficients for the 5 most sensitive nuclides are computed at different periods in the equilibrium cycle, as shown in Figure 18. The sensitivity profiles show noteworthy trends. For example, a large positive sensitivity profile for ^{235}U capture is evident, which leads to a positive effect on reactivity. Whereas, the negative sensitivity profile of ^{238}U capture cross section is again clear: an increase of this reaction cross section will lead to absorption of fast neutrons and decrease the neutron population which will introduce negative reactivity. In Figure 19, the uncertainty contribution of these nuclides to the total uncertainty for BOC is shown. Additionally, a good comparison is observed for UQ using GPT between SERPENT and PERSENT as the two methods show overlapping sensitivity and uncertainty profiles. Slight deviation is observed depending on the energy structure used in the two codes.

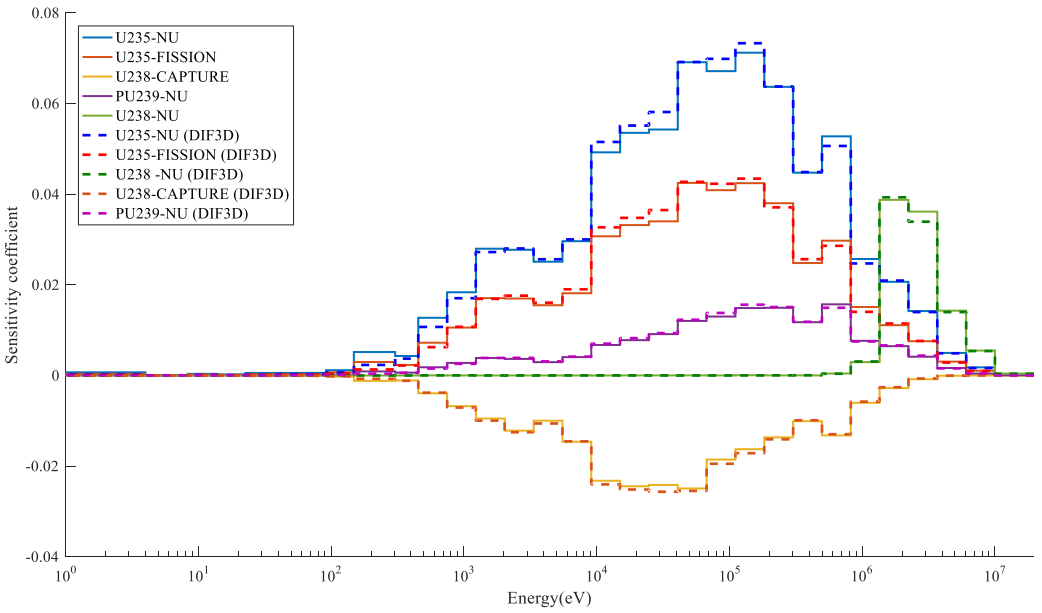

Figure 18: Sensitivity profile for top 5 cross-sections to which keff is most sensitive at BOC (solid lines for SERPENT results, dashed lines for DIF3D results).

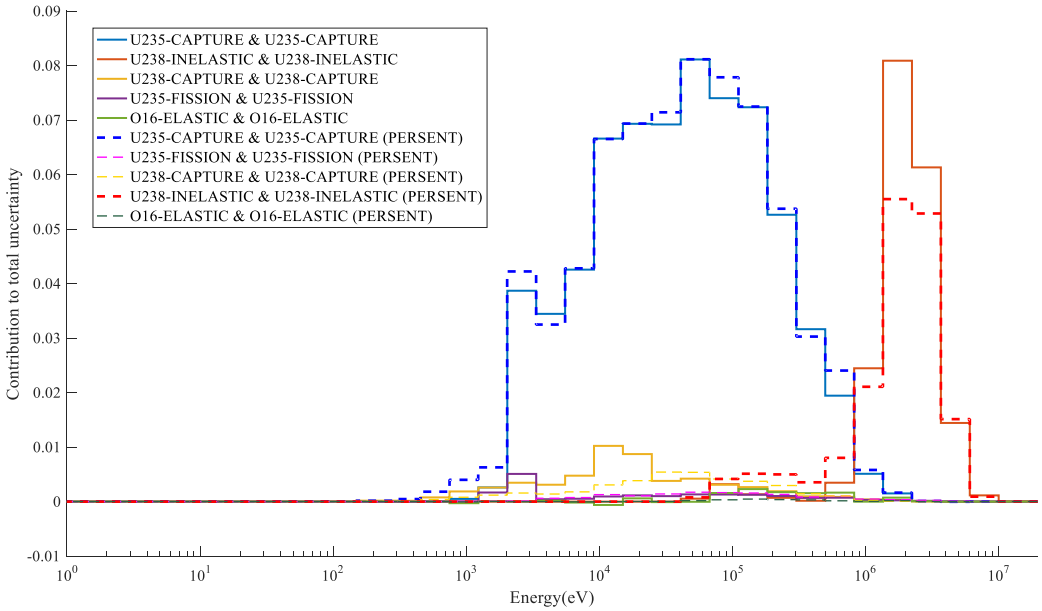

Figure 19: Uncertainty contribution from the main 5 isotopes at BOC. Solid lines for SERPENT results, dashed lines for PERSENT results (solid lines for SERPENT results, dashed lines for DIF3D results).

A substantial amount of uncertainty contribution from ^{235}U capture-^{235}U capture reaction pair is evident in Figure 19. This is not a surprising result considering the high enrichment in the core at BOC. The ^{238}U inelastic-^{238}U inelastic reaction pair provides the next largest contribution. Contribution from the top two nuclide reaction pairs accounts for 85% of the uncertainty in k_{eff} when the respective cross-section was perturbed by 1.01. In addition, there is good comparison between the uncertainty profiles from SERPENT and PERSENT based on the trends observed in Figure 19, although the values are not distinguishable in the lower energy range. This is likely due to the low flux in that region as shown in Figure 13.

5.3.3 UQ&P in Reactivity Feedback

Total uncertainty of each feedback coefficient from perturbations in nuclear data is given in Table 6. Largest uncertainties are observed for the fuel density expansion followed by coolant expansion and Doppler.

Table 6: Total uncertainty of steady state feedback coefficients

	$\Delta\rho$ Doppler	$\Delta\rho$ Fuel	$\Delta\rho$ Coolant	$\Delta\rho$ Structure	$\Delta\rho$ Radial Expansion
$\Delta\rho$ (pcm)	-713.51	-1423.98	-70.51	4513.37	-851.31
Total Uncertainty	**2.51 %**	**9.21 %**	**3.04 %**	**0.44 %**	**1.17 %**

Breakdown of the total uncertainty of neutronic feedback coefficients from Table 6 is provided in Figures 20-23 to show contribution from various reaction channels. A large contribution is observed for fuel density and Doppler reactivity feedback coefficient at BOC composition where majority of the uncertainty is seen to originate from U-238 inelastic scattering in high-energy range above 1 MeV. This can be associated with the significant sensitivity of the feedback coefficients

to the perturbations in U-238 inelastic reaction cross-section and strong reaction channel correlation in this energy range. For core radial expansion and structure feedback (Figs. 6b and 7b, respectively), U-235 fission and capture cross-section become significant in epithermal range. Decreased structural density leads to reduced moderation, increased fission, and addition of uncertainty contribution from U-235. Similarly, expansion of core pitch will increase coolant volume inside the reactor and add negative reactivity.

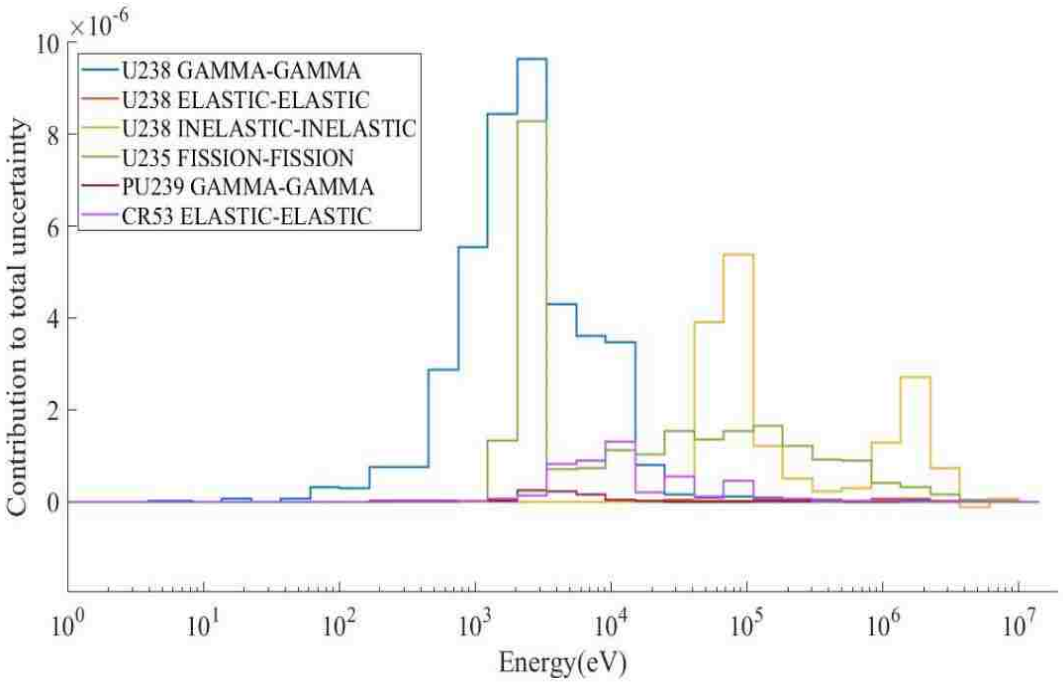

Figure 20: Uncertainty breakdown of Doppler reactivity feedback

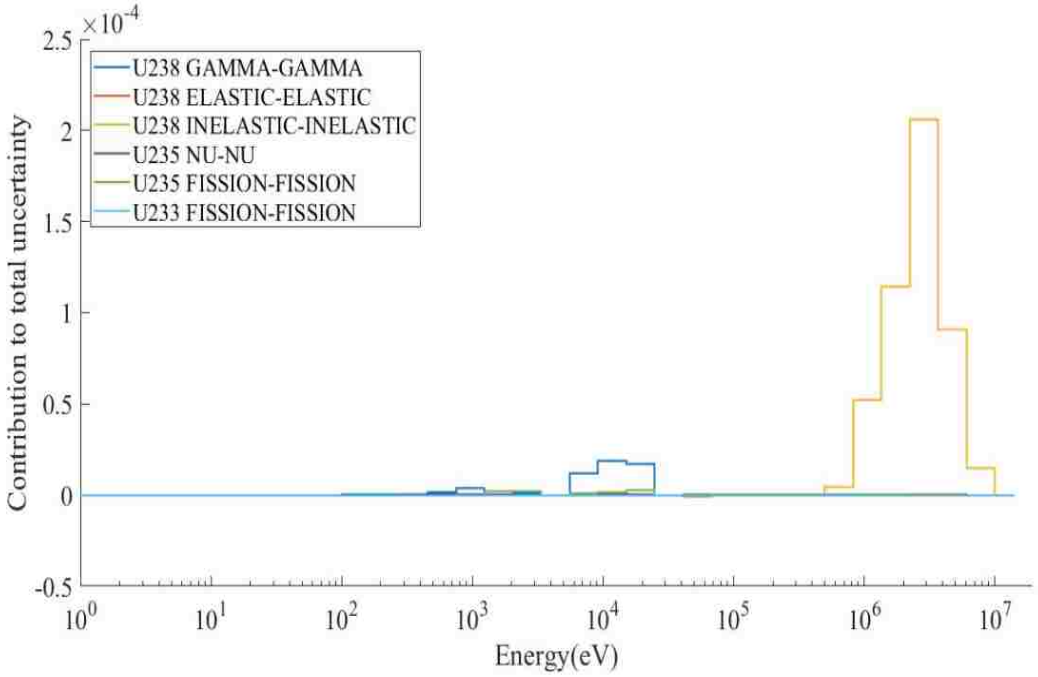

Figure 21: Uncertainty breakdown of radial feedback coefficients

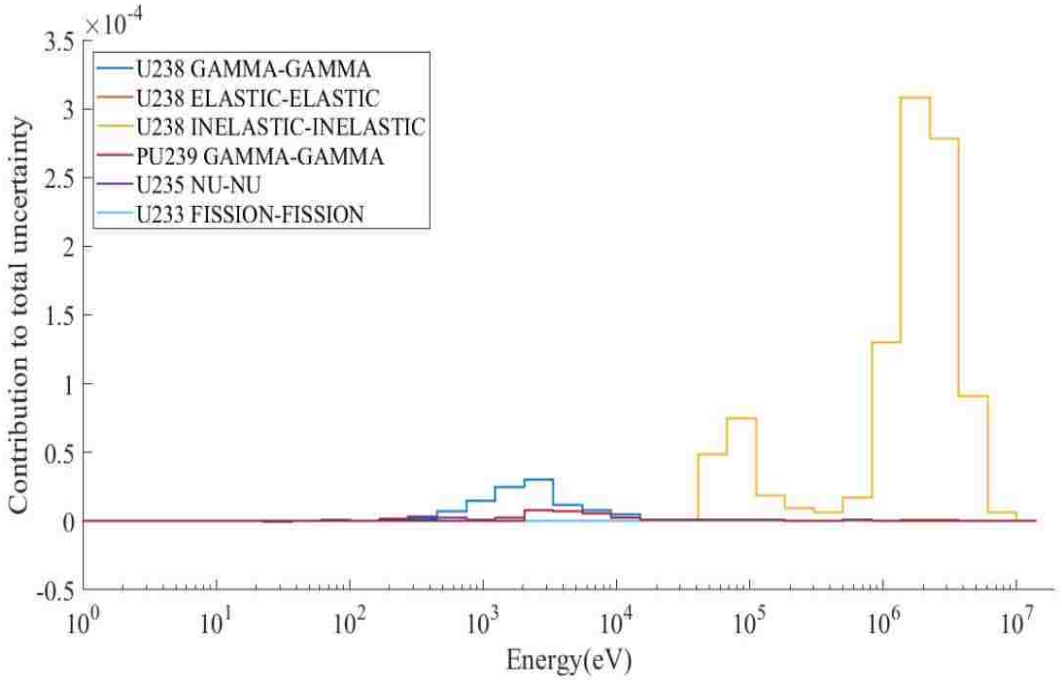

Figure 22: Uncertainty breakdown on fuel and feedback coefficients

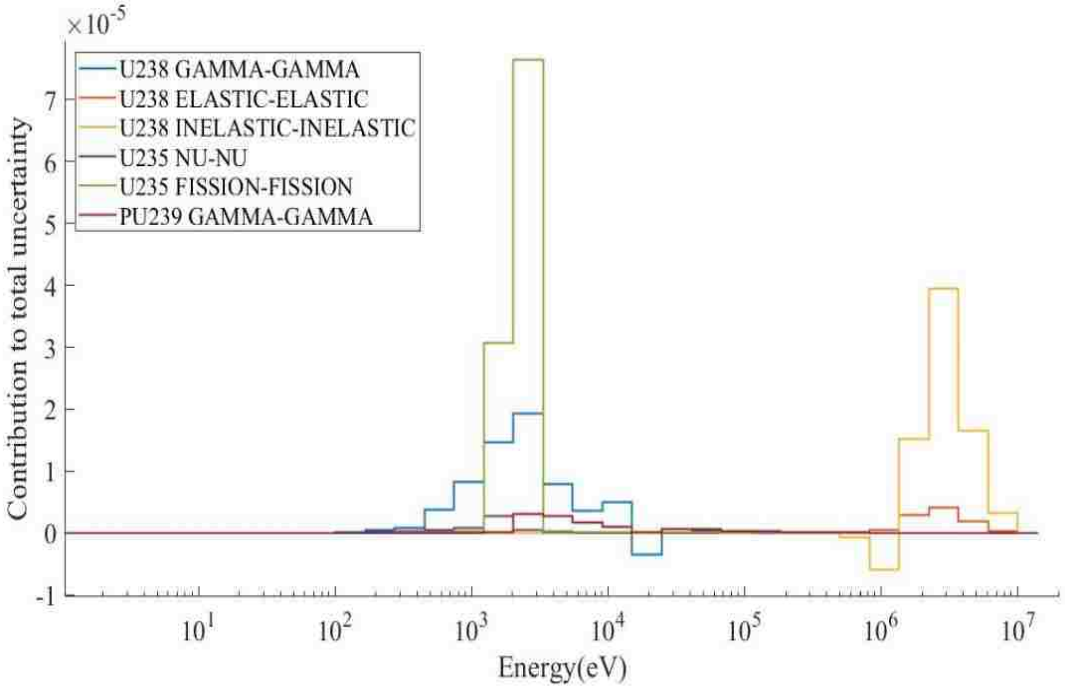

Figure 23: Uncertainty breakdown of structure feedback coefficient

CHAPTER

6

CONCLUSION AND FUTURE WORK

6.1 Concluding Remarks

Uncertainty quantification and sensitivity analysis are key parameters in reactor design. In this work, a method is developed for quantification of nuclear data uncertainties through lead-cooled fast reactors using best estimate methods. The uncertainty and sensitivity profiles are generated using the Monte Carlo code SERPENT with GPT and the ANL code package for fast reactors, ARC, for the equilibrium core composition. Impact of these uncertainties is assessed on core performance and safety parameters including reactivity feedback. It is observed that multiplication factor is most sensitivity to perturbations in ^{235}U-fission cross-section, ^{235}U-ν and ^{238}U-capture cross section. This is followed by ^{239}Pu and ^{238}U-capture cross sections as the fuel experiences burnup. Additionally, at BOC composition, ^{238}U-elastic, ^{238}U-inelastic and ^{238}U-capture cross-sections are identified as top contributors to the total uncertainty in reactivity feedback coefficients.

Furthermore, this work provides a framework for propagation of nuclear data uncertainties through LFR system model described in the next chapter.

6.2 Future Work

In order to propagate nuclear data input uncertainties through transients, uncertainties in feedback coefficients are established. Feedback coefficients can then be perturbed with those standard deviations to evaluate core safety capabilities.

6.2.1 Reactor System Model

In its initial stages, the DLFR system model is envisioned to include a primary heat transfer system and emergency heat removal system (DRACS) driven by natural circulation. The model is generated in the limited, non-commercial version of SAS4A/SASSYS-1, called MiniSAS developed by ANL [14]. MiniSAS is compiled from the same source code as SAS4A/SASSYS-1 while excluding some capabilities such as severe accident modelling [14]. The overall system design is adapted from the sodium fast reactor ABR1000 system for preliminary safety analysis of DLFR [15]. In the current model, coolant flows from hot pool to heat exchangers and is dumped back into cold pool. Primary pumps then feed cold lead through the core extracting heat from the reactor. A once through steam generator is also modelled in the secondary system. In order to make the ABR 1000 model more suitable for LFR system, some design parameters were updated from existing LFR data including core flow rate of 28560 kg/s, coolant inlet temperature at 663.3 K and core power of 500 MW_{th} in nominal state [4]. A more comprehensive list of system specification and coolant flow schematic is provided in Appendix B.

Radial heterogeneity in the reactor core is preserved to some extent by assigning channels to represent the inner and outer core fuel assemblies with varying enrichments. Assembly average power, average coolant flow rate, Doppler feedback coefficient and axial power profiles are specified individually per channel which is represented by a single pin channel model. The fuel

pin is discretized into 10 radial temperature nodes and 20 axial segments. A simple radial expansion model from MiniSAS is incorporated to account for core bowing effect.

6.2.2 Transient Simulation

After establishing steady state, reactivity feedback and temperature increase during the unprotected transient over power (UTOP) accident is evaluated using MiniSAS. The transient is simulated with reactivity insertion of $0.5 over 15 second to represent inadvertent rod withdrawal accident with reactivity ramp. No safety or control rods are envisioned to enter the core during this event. The pumps are expected to operate at full speed with heat transfer occurring via primary loop and DRACS. Remaining parameters were anticipated to be those at nominal state. Peak fuel, clad and coolant temperatures are selected as the quantities to interest to provide an insight into core safety during accidents as shown in Figure 24.

The reactivity ramp during transient increases fuel temperature (Figure 24) but a large negative Doppler is immediately triggered to counter the positive reactivity excursion (Figure 25). Additional negative reactivity feedback from core flowering effect compensates for the remaining positive reactivity inserted during transient. Another main concern during UTOP transient is the fuel peak temperature, which however remains well below the melting point of 3200K for UO_2 fuel.

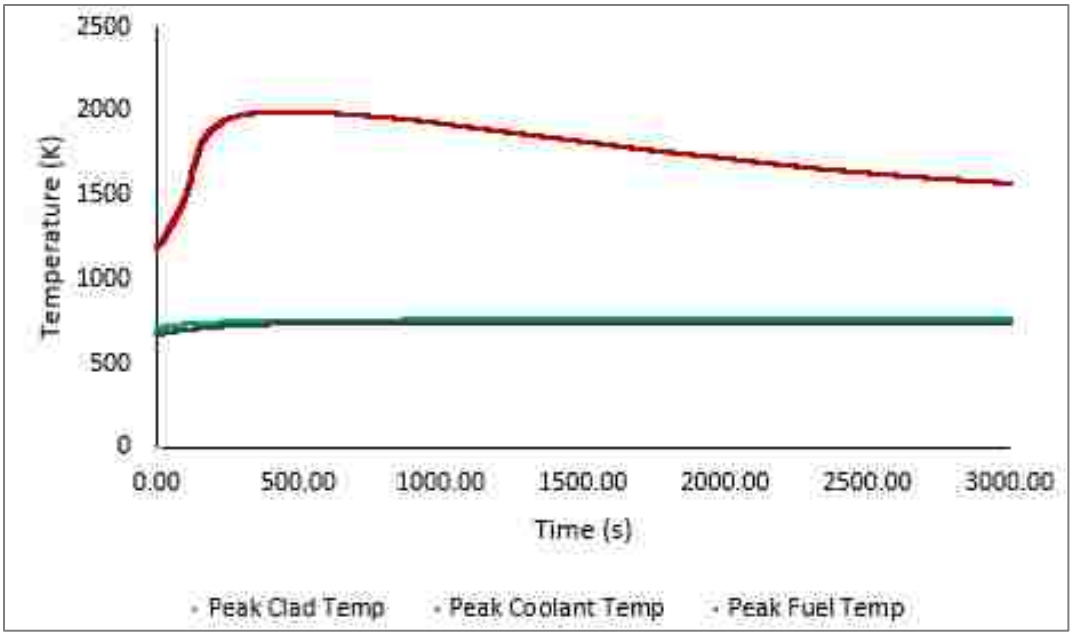

Figure 24: UTOP peak temperatures

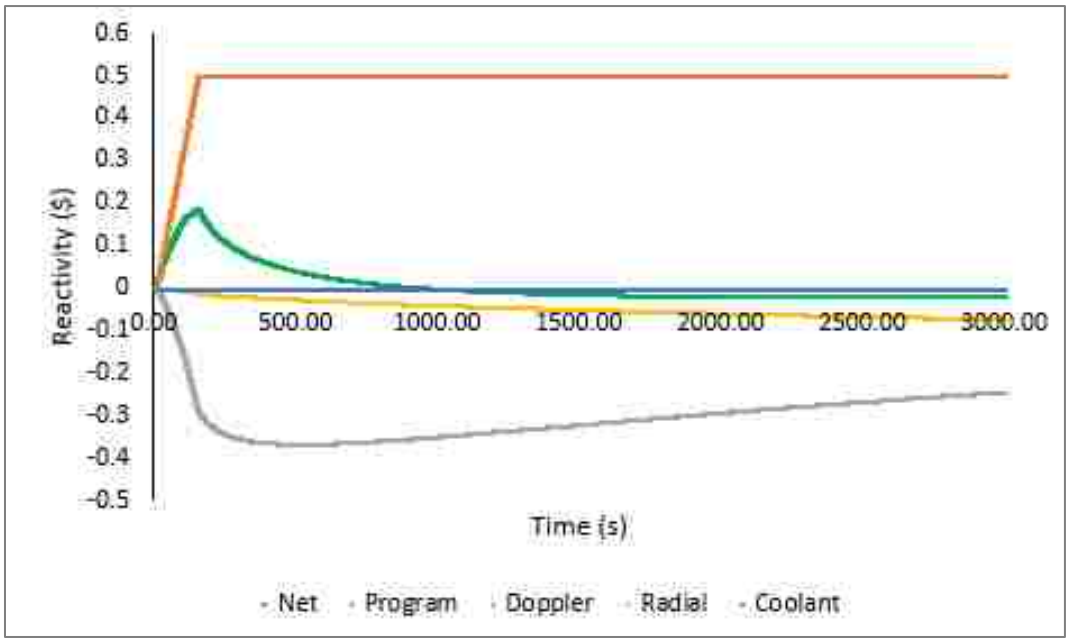

Figure 25: Reactivity feedback observed during transient simulation

For uncertainty quantification of safety parameters, the feedback coefficient uncertainties are expected to be propagated through transients. The adopted propagation methodology can be improved to account for correlated parameters where a change in one type of nuclear data affects multiple reactivity coefficients within different nuclide-reaction uncertainties. Generation of space and energy dependent covariance of feedback coefficient can be achieved by tracking uncertainty quantification of each nuclide-reaction and energy combination.

REFERENCES

1. Alemberti et. al, “Overview of lead-cooled fast reactor activities,” Progress in Nuclear Energy, 77, pp. 300-307 (2013).

2. G.Grosch, “Generation IV Systems,” GIF Portal - Home, (2013)

3. Nuclear Energy Agency. “Handbook on Lead-bismuth Eutectic Alloy and Lead Properties, Materials Compatibility, Thermal-hydraulics and Technologies”. Technical report NEA No. 7268, OECD, 2015

4. “Demonstration Lead-cooled Fast Reactor,” Contract DE-AC02-06CH11357, RT-TR-15-30, Westinghouse Electric Company LLC, March 8, (2016).

5. B. J. Toppel et. al., “The Argonne Reactor Computation (ARC) System,” Technical report, ANL-7332, Argonne National Lab, (1967).

6. M.C. Smith et al. “MC2 -3: Multigroup Cross Section Generation code for Fast Reactor Analysis,” Technical Report ANL/NE-11-41, (2013).

7. J. Leppanen et al. “The SERPENT Monte Carlo code: Status, development and applications in 2013”. Annals of Nuclear Energy, vol. 82, 2015, pp. 142-150.

8. J.M. Ruggieri, et. al., “ERANOS 2.1 : International Code System for GEN IV Fast Reactor Analysis,” *Proceeding of ICAPP*, Nevada USA, (2006).

9. R. Alcouffe et al., “User’s Guide for TWODANT: A Code Package for Two-Dimensional, Diffusion-Accelerated Neutral-Partical Transport,” LA-10049-M, LANL, (1984).

10. K.L. Derstine, “Dif3D: A Code To Solve One-, Two- and Three- Dimensional Finite-Difference Diffusion Theory Problems,” Technical report ANL-82-64, ANL, (April 1984).

11. S.G. Popov et al., “Thermophysical Properties of MOX and UO2 Fuels Including the Effects of Irradiation,” ORNL/TM-2000/351, (July 2000).

12. Del Nevo et al., “Modelling and Analysis of Nuclear Fuel Pin Behavior for Innovative Lead Cooled FBR,” Technical Report ADPFISS-LP2-054, (2014).

13. Lee et al., “Improved Reactivity Worth Estimation of MC2-3/DIF3D in Fast Reactor Analysis,” Proceedings of ANS Sumer Meeting, San Antonio, Texas, (2015).

14. T. H. Fanning et al., “SAS4A/SASSYS-1 Code Improvements for FY 2016,” ANL-ART-75, (2016).

15. N. Stauff et al., “Uncertainty Quantification of ABR Transient Safety Analysis,” Proceedings of ANS Best Estimate Plus Uncertainty (BEPU) International Conference, Lucca, Italy, (2018).

16. R.C. Smith. Uncertainty Quantification. Siam, Philadelphia, 2014.

17. M. Herman et al. “AFCI-2.0 Neutron Cross Section Covariance Library”. Technical report BNL-94830-2011, BNL, March 2011. doi:10.2172/1013530.

18. M.A. Smith et al. “VARI3D & PERSENT: Perturbation and Sensitivity Analysis”. Technical report ANL/NE-13/8, ANL, June 2013.

19. K.F. Laurin-Kovitz and E.E. Lewis. “Variational Nodal Transport Perturbation Theory”. Nuclear Science and Engineering, vol. 123, no. 3, 1996, pp. 369-380.

20. M. Aufiero et al. “A collision history-based approach to sensitivity/perturbation calculations in the continuous energy Monte Carlo code SERPENT”. Annals of Nuclear Energy, vol. 85, 2015, pp. 245-258.

21. B. M. Adams et al., “Dakota, A multilevel Parallel Object-Oriented Framework for Design Optimization, Parameter Estimation, Uncertainty Quantification, and Sensitivity Analysis: version 6.9 Manual,” (2018).

22. N. Stauff et al., “Uncertainty Quantification of ABR Transient Safety Analysis-nuclear data uncertainties,” Proceedings of ANS Best Estimate Plus Uncertainty (BEPU) International Conference, Lucca, Italy, (2018).

23. G. Grasso et al., “The Core Design of ALFRED, A Demonstrator for the European Lead cooled Reactors,” Nuclear Engineering and Design, 278, pp. 287-301 (2014).

24. F. Bostelmann et al. “Benchmark for Uncertainty Analysis in Modelling (UAM) for Design, Operation and Safety Analysis of SFRs”. March 2017.

APPENDICES

Appendix A

System model specifications for the currently DLFR system in Mini SAS

System Components	Description
Coolant Flow rate	28560 kg/s
Coolant inlet	663K
Fuel/Coolant Type	Oxide/Lead
Core Channels	2 channels: IC and OC
Heat Exchanger (HX)	4 identical HX – 1 is modelled in SAS
Steam Generator	Once through SG
Pump	Normalized pump head vs. time provided for the intermediate and primary pumps
Direct Reactor Auxiliary Cooling System (DRACS)	Emergency cooling system
Beta values	8.1430E-05 5.9311E-04 5.0653E-04 1.1955E-03 7.0362E-04 2.5761E-04

Appendix B

33 energy group stricture adapted with MCC-3.1, SERPENT-2.0 and COMMARA-2.0 with energies in eV

Group	MCC-3.1 (ANL)	SERPENT-2.0	COMMARA-2.0
1	1 1.4191E+07	1.964033E+07	1.964033E+07
2	2 1.0000E+07	1.000000E+07	1.000000E+07
3	3 6.0653E+06	6.065307E+06	6.065307E+06
4	4 3.6788E+06	3.678794E+06	3.678794E+06
5	5 2.2313E+06	2.231302E+06	2.231302E+06
6	6 1.3534E+06	1.353353E+06	1.353353E+06
7	7 8.2085E+05	8.208500E+05	8.208500E+05
8	8 4.9787E+05	4.978707E+05	4.978707E+05
9	9 3.0197E+05	3.019738E+05	3.019738E+05
10	10 1.8316E+05	1.831564E+05	1.831564E+05
11	11 1.1109E+05	1.110900E+05	1.110900E+05
12	12 6.7379E+04	6.737947E+04	6.737947E+04
13	13 4.0868E+04	4.086771E+04	4.086771E+04
14	14 2.4787E+04	2.478752E+04	2.478752E+04
15	15 1.5034E+04	1.503439E+04	1.503439E+04
16	16 9.1188E+03	9.118820E+03	9.118820E+03
17	17 5.5308E+03	5.530844E+03	5.530844E+03
18	18 3.3546E+03	3.354626E+03	3.354626E+03
19	19 2.0347E+03	2.034684E+03	2.034684E+03
20	20 1.2341E+03	1.234098E+03	1.234098E+03
21	21 7.4852E+02	7.485183E+02	7.485183E+02
22	22 4.5400E+02	4.539993E+02	4.539993E+02
23	23 2.7536E+02	3.043248E+02	3.043248E+02
24	24 1.6702E+02	1.486254E+02	1.486254E+02
25	25 1.0130E+02	9.166088E+01	9.166088E+01
26	26 6.1442E+01	6.790405E+01	6.790405E+01
27	27 3.7267E+01	4.016900E+01	4.016900E+01
28	28 2.2603E+01	2.260329E+01	2.260329E+01
29	29 1.3710E+01	1.370959E+01	1.370959E+01
30	30 8.3153E+00	8.315287E+00	8.315287E+00
31	31 3.9279E+00	4.000000E+00	4.000000E+00
32	32 5.3158E-01	5.400000E-01	5.400000E-01
33	33 4.1746E-01	1.000000E-01	1.000000E-01

Appendix C

Sensitivity and uncertainty analysis for DLFR fuel assembly and 2D core model results are presented in this section. BOL/BOC/EOC/EOC refer for beginning of life, beginning of cycle, end of cycle, and end of life, respectively.

Inner Core Assembly BOL

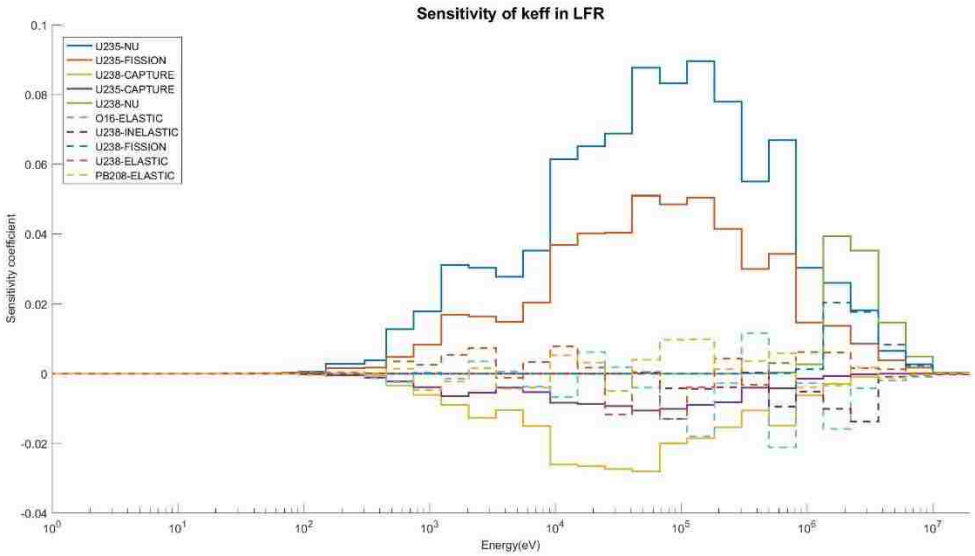

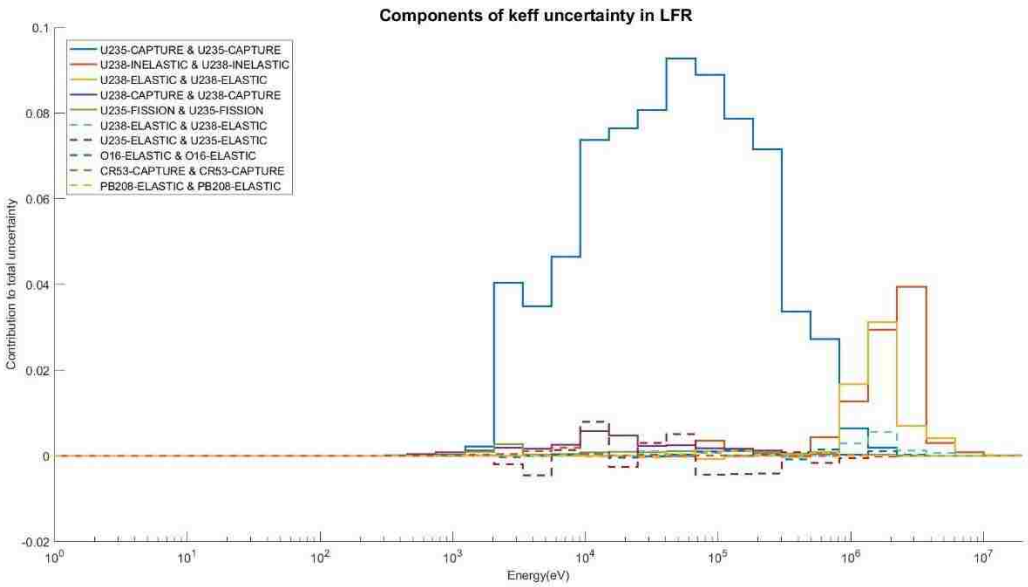

Outer Core Assembly BOL

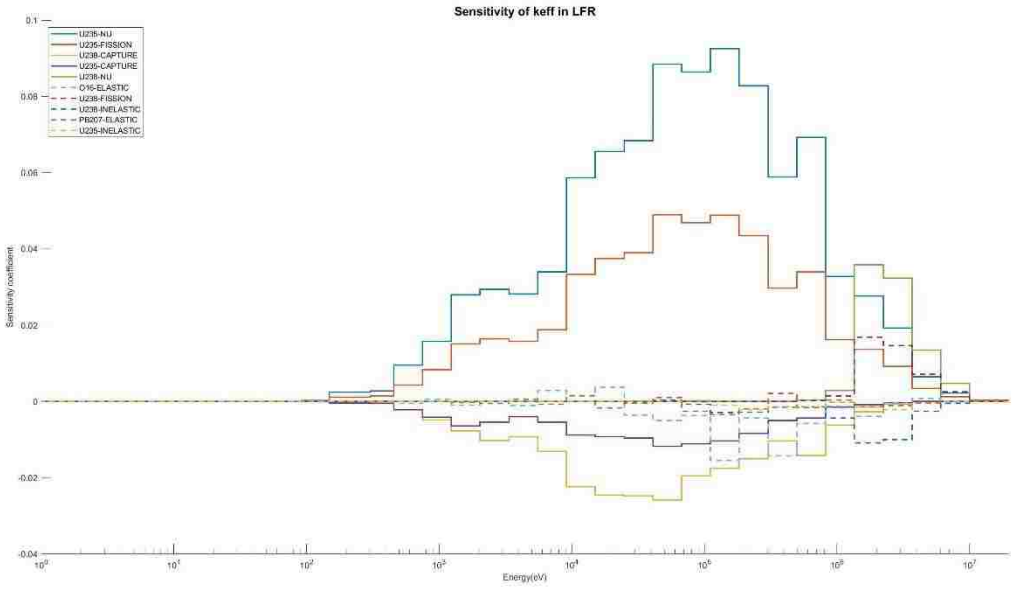

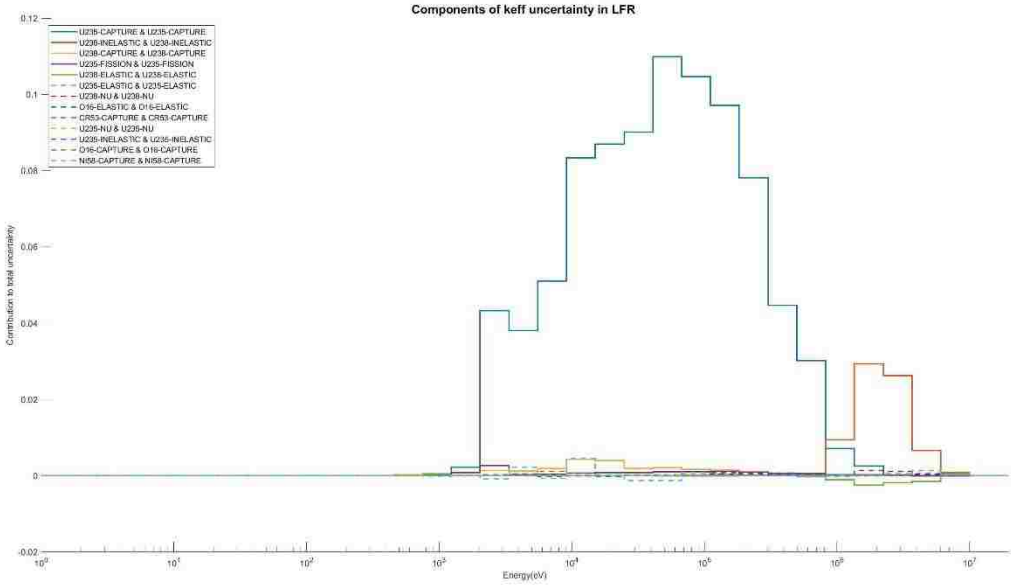

Outer Core Assembly BOC

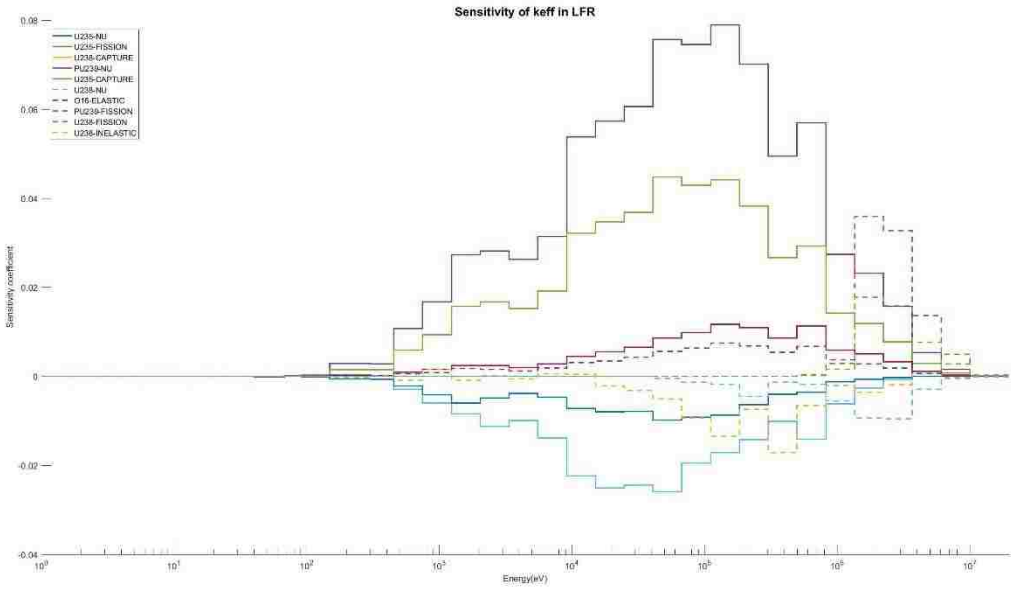

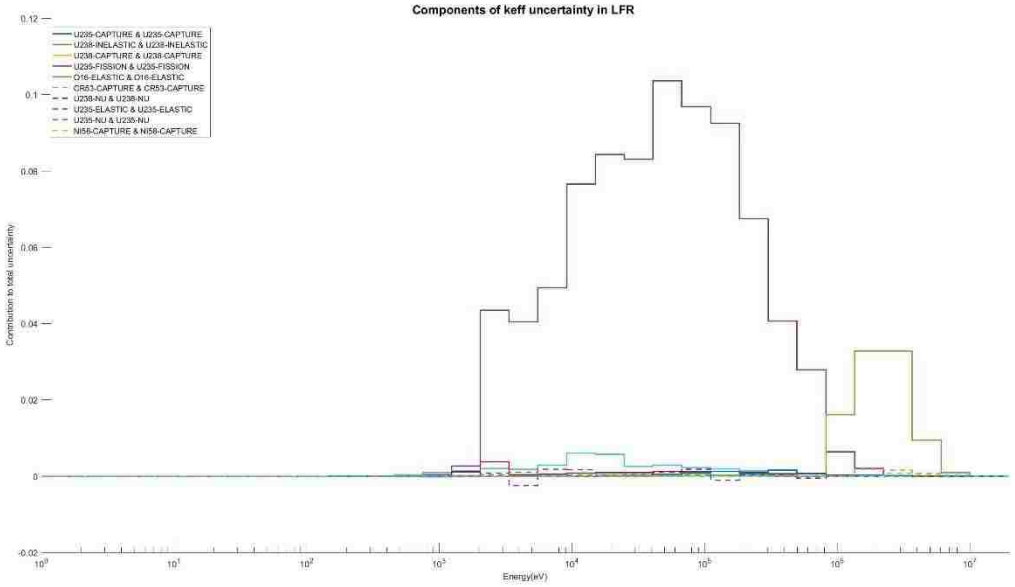

Inner Core Assembly EOC

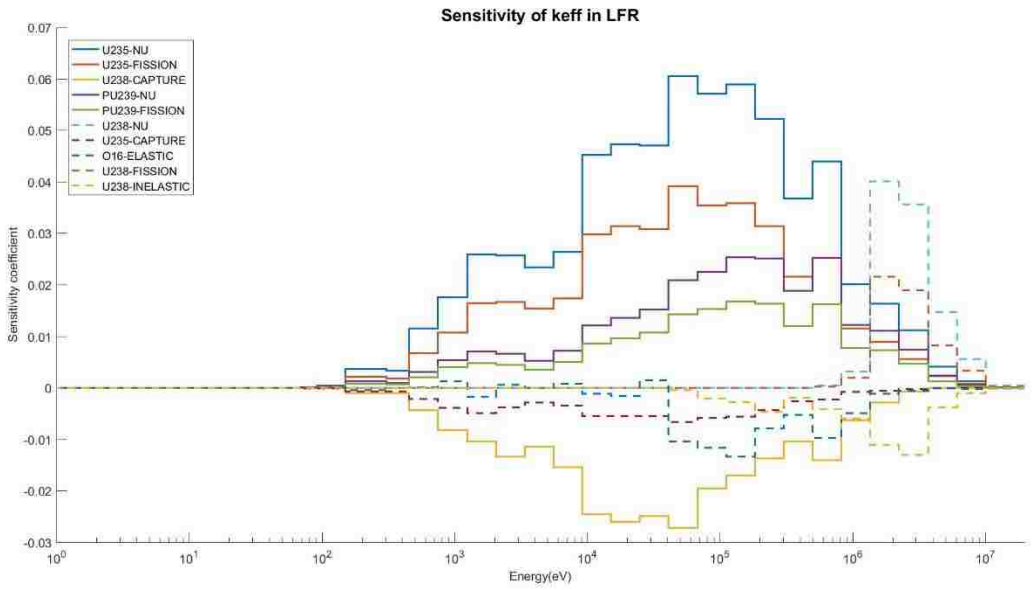

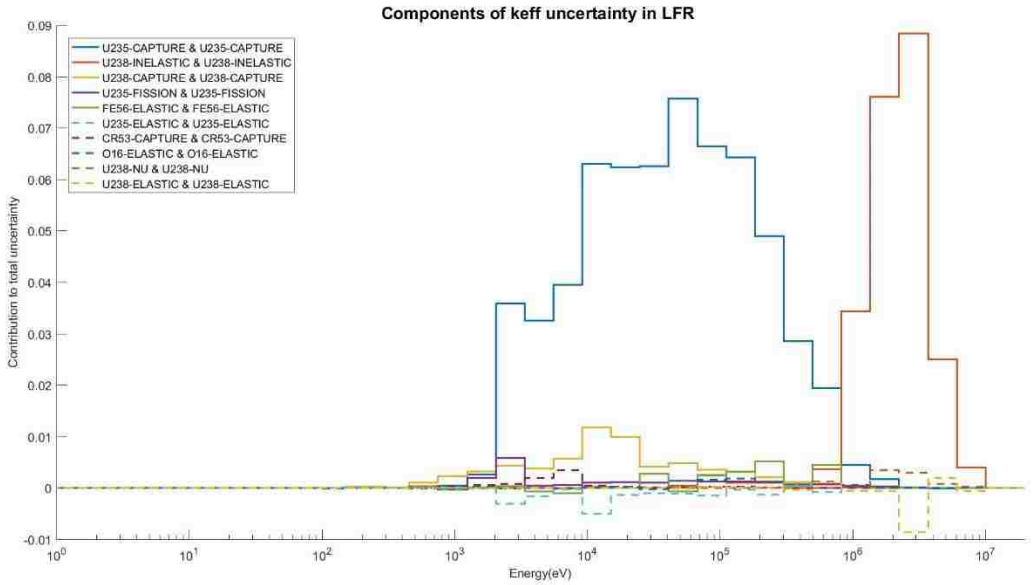

Outer Core Assembly EOC

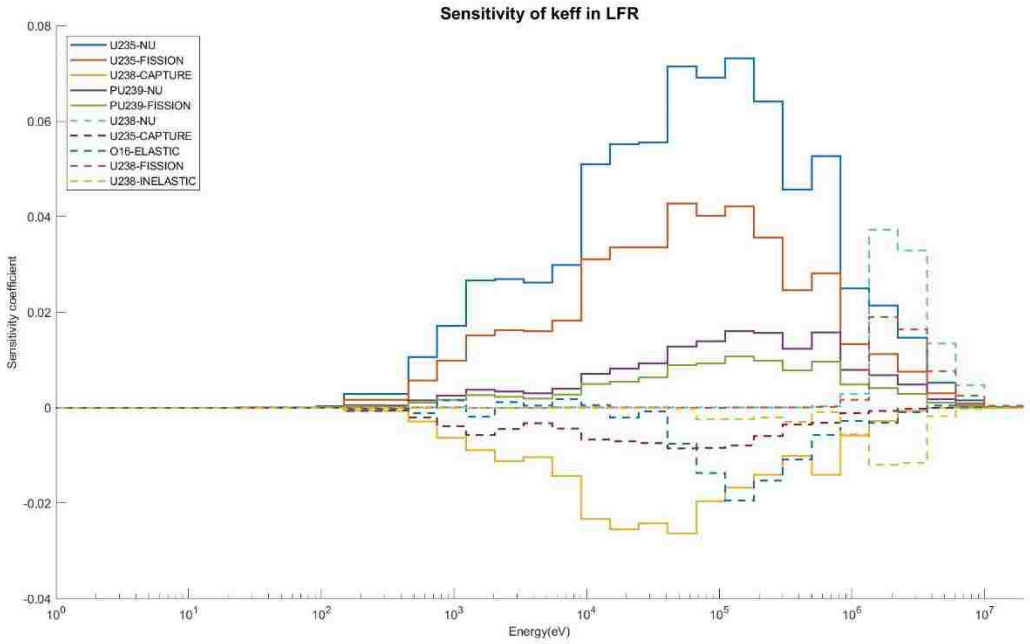

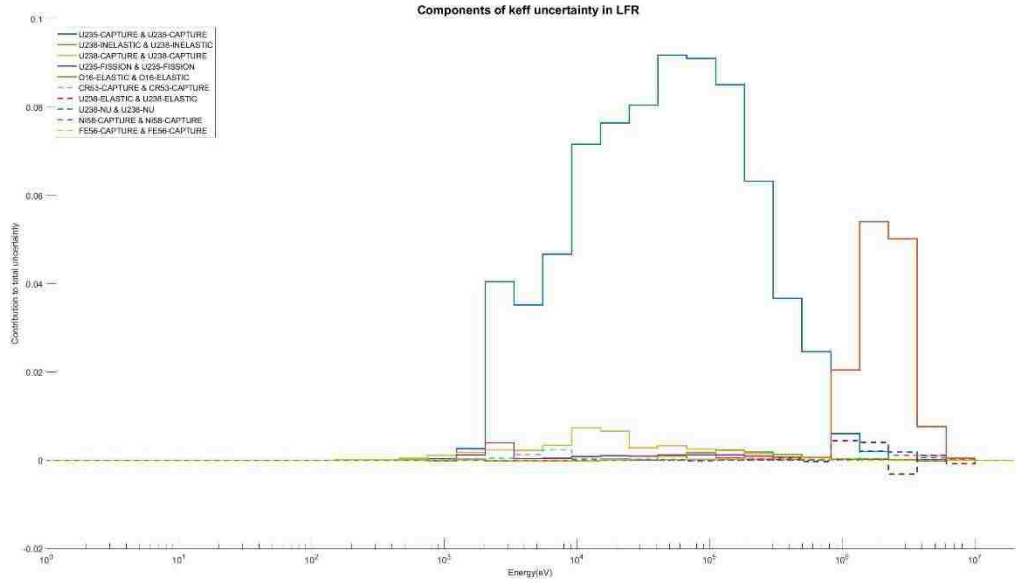

Inner Core Assembly EOL

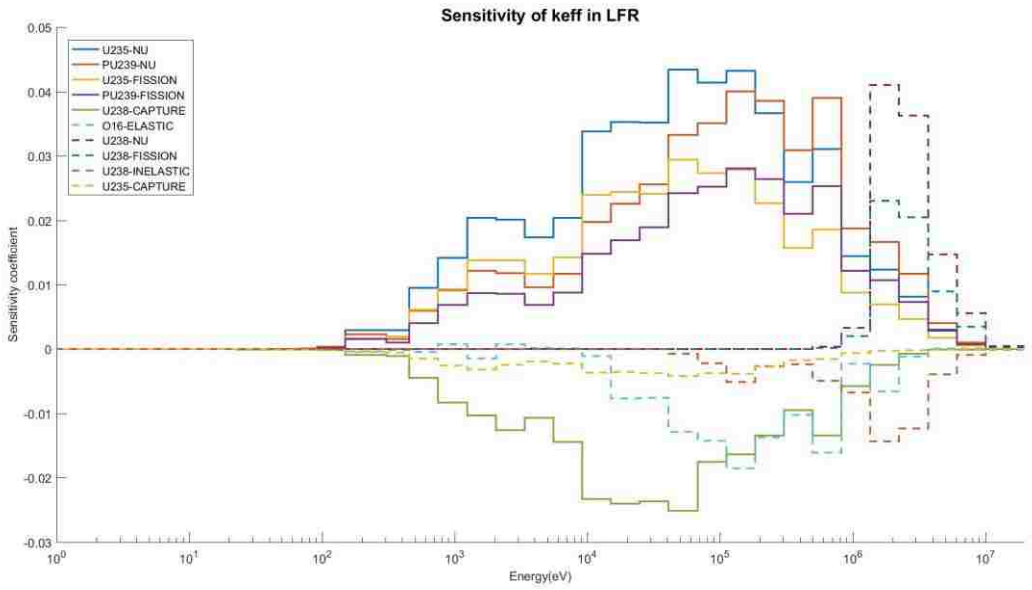

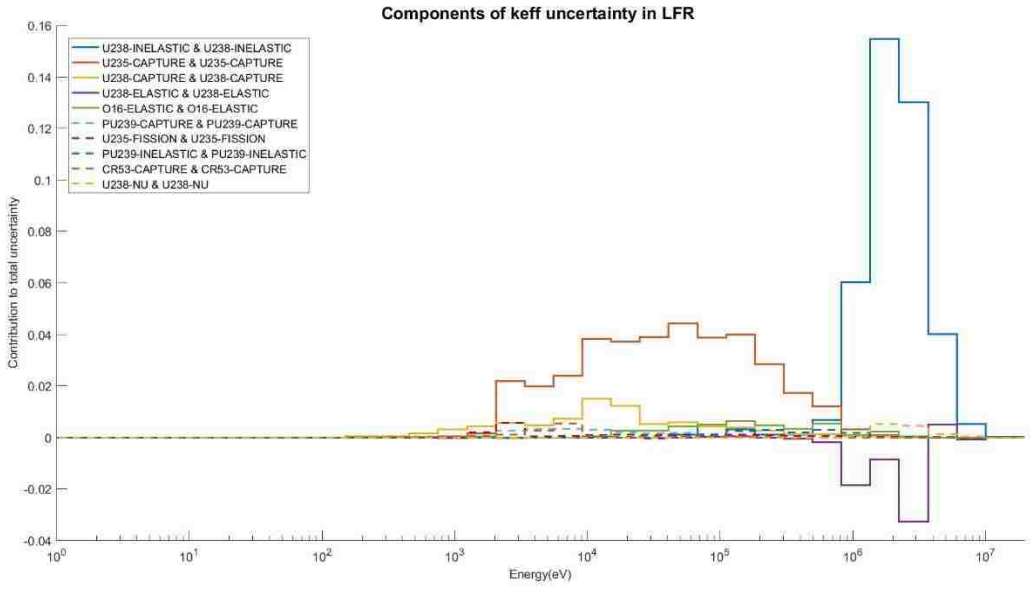

Outer Core Assembly EOL

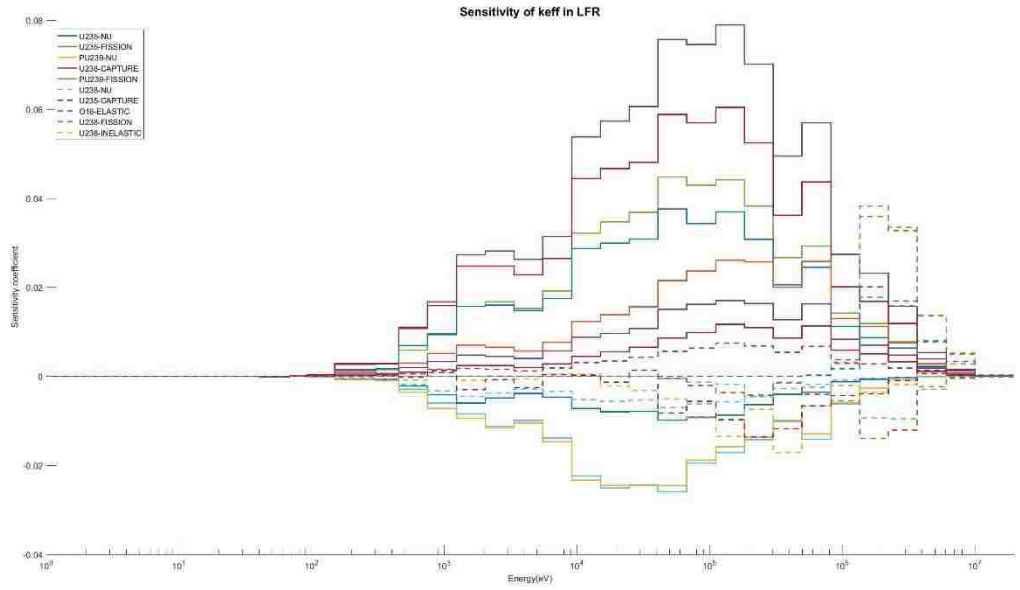

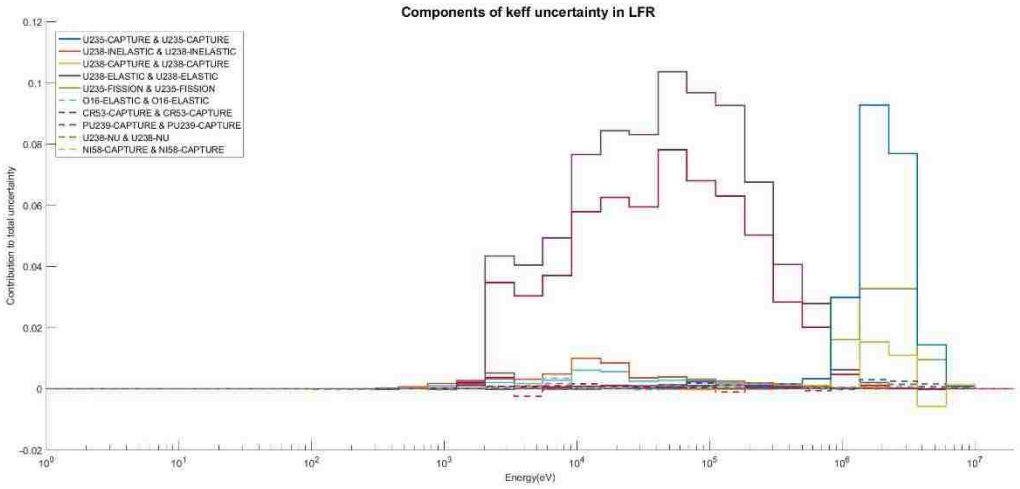

2D Core at BOL

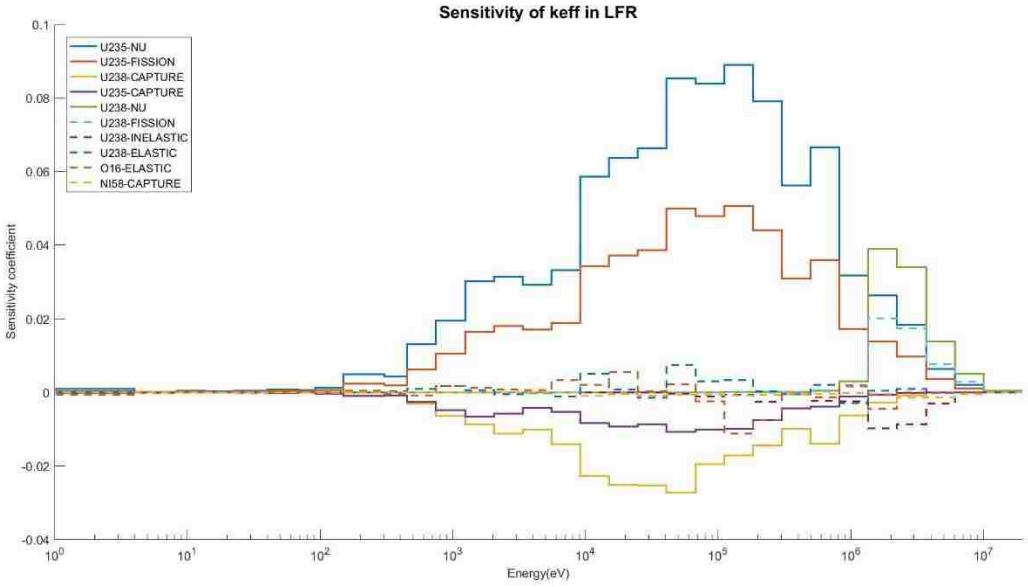

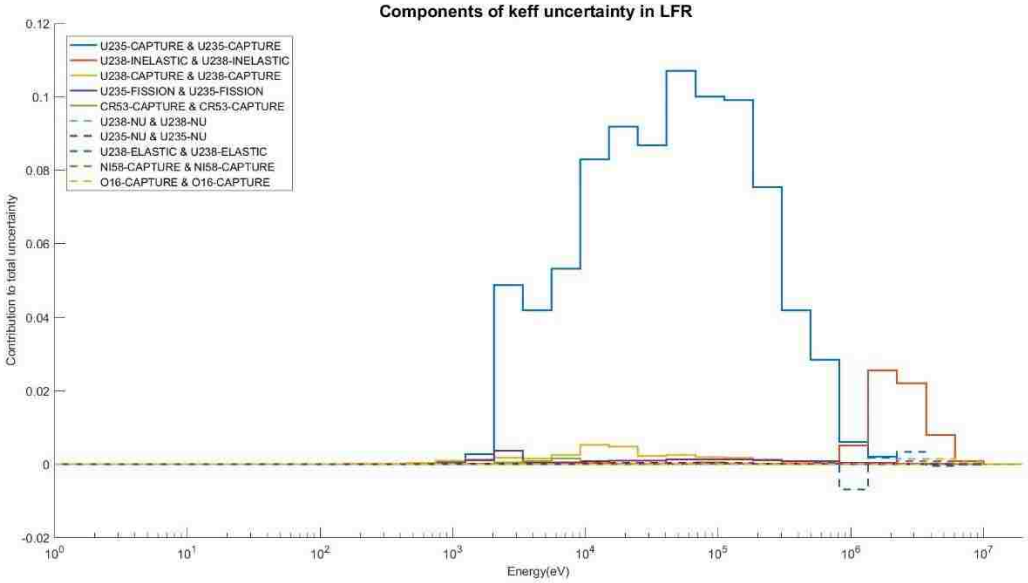

2D Core at EOC

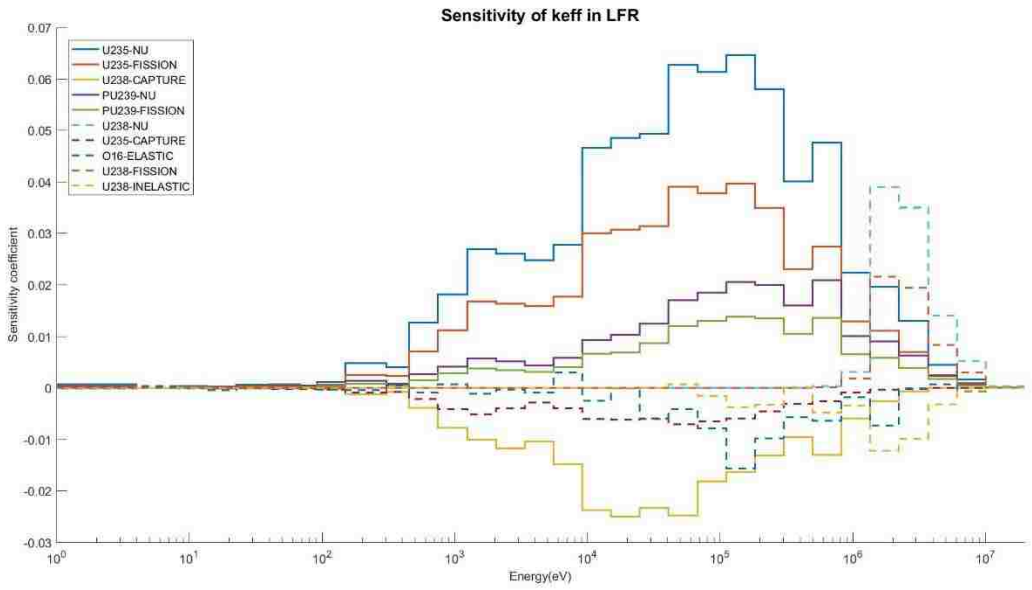

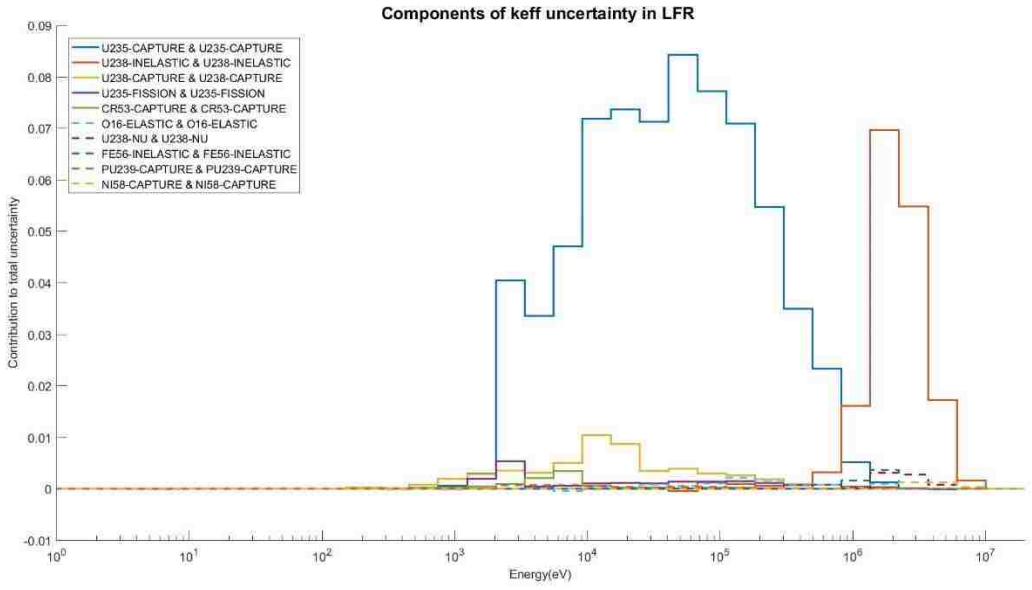

2D Core at EOL